# Firn on ice sheets

Amory, Charles; Buizert, Christo; Buzzard, Sammie; Case, Elizabeth; Clerx, Nicole; Culberg, Riley; Lhermitte, Stef; de Roda Husman, Sophie; Wouters, Bert; More Authors

**DOI**
10.1038/s43017-023-00507-9

**Publication date**
2024

**Document Version**
Final published version

**Published in**
Nature Reviews Earth and Environment

**Citation (APA)**
Amory, C., Buizert, C., Buzzard, S., Case, E., Clerx, N., Culberg, R., Lhermitte, S., de Roda Husman, S., Wouters, B., & More Authors (2024). Firn on ice sheets. *Nature Reviews Earth and Environment*, *5*(2), 79-99. https://doi.org/10.1038/s43017-023-00507-9

nature reviews earth & environment

https://doi.org/10.1038/s43017-023-00507-9

Review article

Check for updates

# Firn on ice sheets

The Firn Symposium team*

**Abstract**

Most of the Greenland and Antarctic ice sheets are covered with firn — the transitional material between snow and glacial ice. Firn is vital for understanding ice-sheet mass balance and hydrology, and palaeoclimate. In this Review, we synthesize knowledge of firn, including its formation, observation, modelling and relevance to ice sheets. The refreezing of meltwater in the pore space of firn currently prevents 50% of meltwater in Greenland from running off into the ocean and protects Antarctic ice shelves from catastrophic collapse. Continued atmospheric warming could inhibit future protection against mass loss. For example, warming in Greenland has already contributed to a 5% reduction in firn pore space since 1980. All projections of future firn change suggest that surface meltwater will have an increasing impact on firn, with melt occurring tens to hundreds of kilometres further inland in Greenland, and more extensively on Antarctic ice shelves. Although progress in observation and modelling techniques has led to a well-established understanding of firn, the large uncertainties associated with meltwater percolation processes (refreezing, ice-layer formation and storage) must be reduced further. A tighter integration of modelling components (firn, atmosphere and ice-sheet models) will also be needed to better simulate ice-sheet responses to anthropogenic warming and to quantify future sea-level rise.

**Sections**

Introduction

Formation and properties of firn

Firn observations

Firn modelling

The changing ice-sheet and ice-shelf firn

Summary and future perspectives

*A list of authors and their affiliations appears at the end of the paper. e-mail: nander.wever@slf.ch

## Introduction

Firn is snow that is more than 1 year old, which has not yet been compacted fully into glacial ice under its own weight. The thickness of the firn layer ranges from several to over 100 metres thick over the ice sheets of Greenland and Antarctica[1], and its composition and appearance are determined by the surface climate[2–4]. Snowfall, surface melt, wind and temperature all modulate the firn, on seasonal and interannual timescales. Firn covers ~99% of the Antarctic[5,6] and ~90% of the Greenland[7] ice-sheet surface. The firn layer, which has an interconnected, air-filled pore space, acts as a sponge, enabling the percolation, retention and refreezing of surface meltwater (Fig. 1). As such, ~50% of Greenlandic and almost all Antarctic surface meltwater refreezes in the firn[8–10], moderating the contribution of ice sheets to sea-level rise.

Anthropogenic warming over the ice sheets, combined with natural variability in temperature and snowfall, is greatly changing the firn layer on Greenland and Antarctica. Because of warming and increased melting in Greenland, firn thickness has reduced by 1–1.5 m since 1980 (refs. 2,3), reducing pore space by ~5% on average over the ice sheet[3,11]. In Antarctica, decadal variability in firn thickness dominates the observed firn thickness change, leading to both regional growth and decay of the firn across the ice sheet[2,4,12].

These changes have marked implications. For example, the annual production of surface meltwater in Greenland has increased by about 40% since the 1990s (ref. 13). The percolation and refreezing of this meltwater caused ice slabs within the firn to expand by 37–44% between 2012 and 2018 (ref. 14). These ice slabs are likely to reduce the buffering capacity and enhance direct runoff, increasing vulnerability to mass loss. Concurrently, the expansion of firn aquifers[15–17] due to increased surface meltwater production is similarly expected to influence Greenland ice-sheet behaviour, although to an unknown extent[18]. Likewise, the decrease in firn air content (FAC) on certain Antarctic ice shelves has allowed water to collect in crevasses, driving and preconditioning the collapse of these floating ice shelves by hydrofracturing. However, increased snowfall during the twentieth century has led to firn mass gain in parts of Antarctica and in the interior of the Greenland ice sheet, partly offsetting firn loss elsewhere on both ice sheets. In all future scenarios with continued anthropogenic warming, the temperature increase over the ice sheets will generally lead to increased precipitation[19], including a shift from snowfall to rainfall[20,21], and increased surface melt[22,23]. Therefore, further changes in the firn are expected for both ice sheets.

Quantifying these observed and projected changes in firn and ice-sheet mass requires accurate characterization of both the microstructural properties and bulk behaviour of the entire firn layer. The firn layer mass, density and thickness vary with time, because they are affected by snowfall, melt and compaction. This variation makes it complicated to derive the mass change of the underlying ice sheets at high spatial and temporal resolution from changes in surface elevation, which is monitored by airborne or satellite altimetry. A solid understanding of firn dynamics is thus needed to accurately interpret any observed changes, which is especially critical given ongoing anthropogenic warming. This knowledge is also crucial to derive records of past atmospheric composition and conditions from air bubbles trapped in glacial ice after the firn compacted beyond the pore close-off. These bubbles act as pivotal records of past atmospheric composition, which are key to understanding future changes, making it even more vital to understand firn processes.

In this Review, we provide an overview of existing knowledge of firn in Greenland and Antarctica, and argue for the need to better understand how firn responds to rapid atmospheric warming. We begin by outlining the formation and properties of firn. We follow with an overview of observational techniques that have revealed changes in the firn layer. We then discuss modelling techniques, which can test the understanding of the physical processes and provide insight on the future state of the firn layer. Last, we summarize observed and projected changes in firn, and outline the major challenges, opportunities and directions for future research.

## Formation and properties of firn

The existence and appearance of firn on an ice sheet (Fig. 1) depend on the surface climate. Temperature, precipitation and wind all determine the amount of snow added to the glacier surface, the amount of surface melt percolating into the firn, and the rate of firn compaction. Firn is characterized in terms of its physical properties, for example density, grain size, microstructure and temperature, which, in turn, determine its mechanical strength and permeability. The firn structure also controls the flow of liquid water through the firn. The impact of atmospheric forcing on the firn layer, the firn properties and firn hydrology are now discussed.

### Atmospheric forcing

Atmospheric forcing consists of mass and energy exchange between the atmosphere and the firn. It determines both the properties of the firn and the rate at which these properties change over time. The atmosphere provides mass at the firn surface through solid and liquid precipitation, condensation and wind deposition. Mass loss occurs through sublimation, evaporation, wind erosion, and melt- or rainwater runoff into the englacial drainage system or at the ice-sheet edges. These mass fluxes together constitute the local (or specific) surface mass balance (SMB). This value can be integrated over the ice sheet to obtain the ice-sheet SMB[24]. Areas with positive or negative local SMB form the accumulation zone and ablation zone, respectively. There are two distinct regions with negative local SMB that can be identified: first, regions with large runoff following surface melt (such as ice-sheet edges and melt-induced blue-ice areas); second, windy areas in which mass loss due to surface sublimation and wind erosion exceeds accumulation (wind-induced blue-ice areas)[6].

Firn–atmosphere energy exchange consists of turbulent fluxes of sensible and latent heat, and of fluxes of thermal and solar radiation. When the sum of these fluxes, which comprises the surface energy balance[24], is positive, the surface heats up, and when the melting point is reached, surface meltwater forms. Surface melt is largely driven by shortwave radiation and sensible heat, with sensible and latent heat having reduced contributions at increased elevation[25]. The net cloud radiative effect provides second-order modulation of the surface energy balance, depending on cloud thickness, altitude and season[26,27]. Turbulent fluxes increase with increasing aerodynamic roughness length, a parameter determined by the spatial distribution of surface roughness elements and the orientation of the wind with respect to these roughness elements. For example, erosional features (sastrugi) in high wind areas (such as wind scour zones) can cause the aerodynamic roughness length to be several orders of magnitude higher than in smooth blue-ice areas[28].

In most of Antarctica, and the interior of Greenland, surface melt is rare, and the local SMB and firn thickness variations are dominated by snowfall, compaction and their seasonal[12] and decadal[29] variability. Currently, seasonal and decadal firn thickness variations remain of similar magnitude in Greenland and Antarctica[4]. Variations in snowfall are influenced by large-scale atmospheric modes, such as the El Niño Southern Oscillation[30] and Southern Annular Mode[29,31,32] in Antarctica, and the North Atlantic Oscillation in Greenland[2,33,34].

Generally, meltwater can be locally retained within a firn layer if the climatological ratio of surface melt over snow accumulation (MOA) is less than ~0.7 (ref. 35). Above this value, meltwater runs off laterally (parallel to the slope) or starts ponding, reducing FAC. Areas with MOA > 0.7 are limited to lower elevations in Greenland, whereas in Antarctica, such areas are localized and occur mostly on ice shelves, which subsequently disintegrate in the northern Antarctic Peninsula. Additionally, the melt extent in Antarctica covers on average 11% of the ice-sheet area[36], concentrated at the margins and the floating ice shelves (Fig. 2a–c). In Greenland (Fig. 2d–f), surface melt extends into the interior, especially in the south, covering 15–20% of the sheet ice[37].

Trends and variations in surface melt are caused by changes in air temperature, cloud cover, snowfall and erosion[38–40], and other processes that influence the surface energy balance, especially through modulation of surface albedo[39]. The presence of liquid water at the surface of the firn layer, together with the associated grain growth[41], decreases the surface albedo (Fig. 1a). In turn, this increases the absorption of solar radiation in the firn, causing more heating and melt to occur. Where the firn is entirely eroded or sublimated off, darker bare ice, which has a lower albedo, is exposed at the surface (Fig. 1a). This strong, positive melt–albedo feedback currently accounts for more than half of the surface melting in Greenland[42] and Antarctica[43] and is likely to remain at least as important in the future[22,44].

The state of the firn layer is governed by the atmosphere; therefore, anomalous large-scale atmospheric conditions and atmospheric extremes have a large impact on its structure and evolution. Anomalous atmospheric circulation and even one-off weather extremes can affect firn properties in a large area for decades, for example through the formation and thickening of ice layers in the firn[45–47]. Since the end of the 1990s, the increasing occurrence of atmospheric blocking favouring warmer and more anticyclonic (drier) conditions over Greenland[48] has led to record surface runoff above 500 Gt yr$^{-1}$ and 600 Gt yr$^{-1}$ in 2012 and 2019, respectively[49,50], and an inland expansion of low-permeability ice slabs by 13,400–17,600 km$^2$ or 37–44% between 2012 and 2018 (ref. 14). Atmospheric rivers are another example of atmospheric conditions with a strong effect on the firn layer[51,52]. Despite being rare, these long, narrow bands of high water vapour content from subtropical to (sub-)polar latitudes account for most of the annual precipitation in some ice-sheet regions[52,53]. In Greenland, atmospheric rivers mostly contributed to the increase in mass loss that has occurred since 2000 (refs. 52,54), with SMB losses generally exceeding moderate SMB gains. Across most of the Antarctic ice sheet, atmospheric rivers are the primary driver of the most extreme snowfall events[55,56] and locally control the interannual variability of precipitation, the dominant SMB term at the ice-sheet scale.

In addition to the challenges in modelling firn itself, a major uncertainty in simulating present and future ice-sheet firn stems from uncertainties associated with atmospheric forcing, including the role of clouds[20,22,57], extreme weather events[52,53,55], biases in climate models[58,59], and circulation changes[60,61].

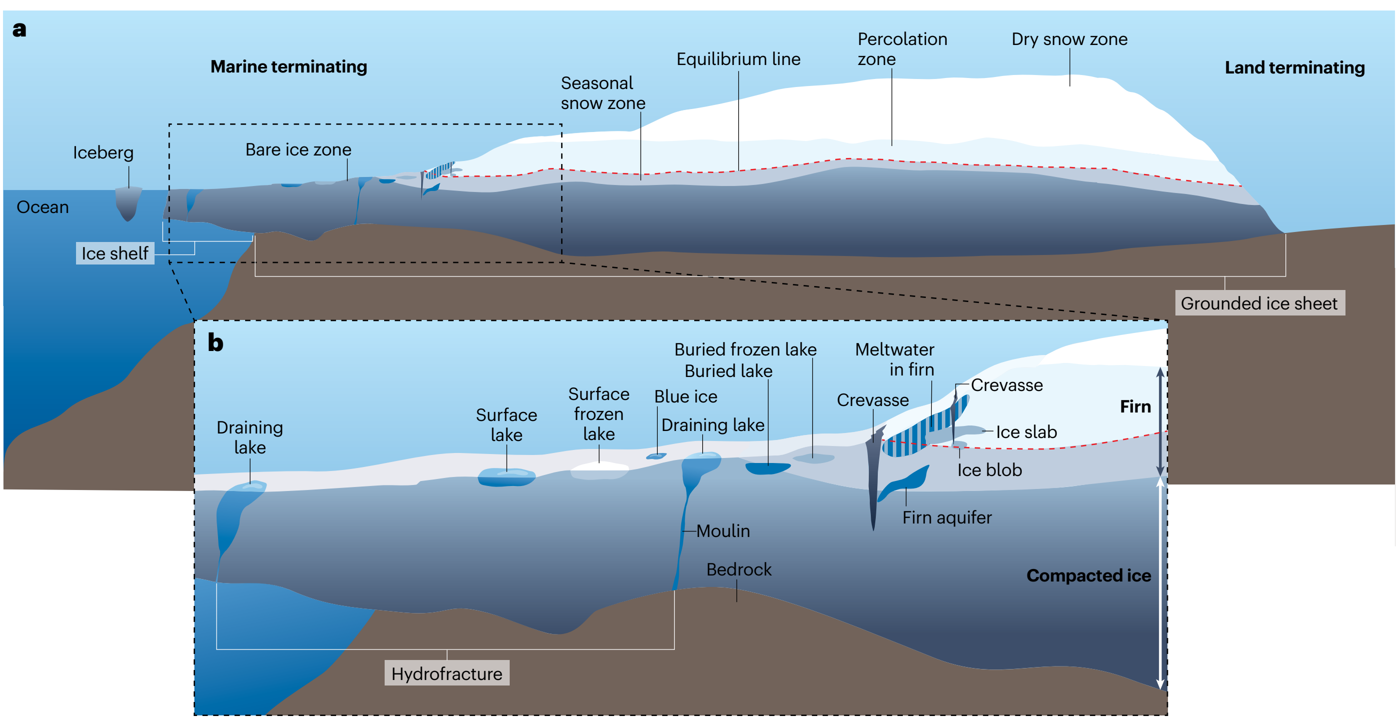


**Fig. 1 | Schematic representation of important ice-sheet features. a**,**b**, Full ice sheet (**a**) and a zoom in showing surface and hydrological features (**b**), including liquid water (blue), ice features (grey), crevasses (black) and bedrock under the ice (brown). Large parts of the Antarctic ice sheet terminate in ice shelves (left-hand side of panel **a**) whereas most of the ice sheet on Greenland terminates over land (right-hand side of panel **a**). The equilibrium line (red dashed line) separates the accumulation zone (including the dry snow zone and percolation zone) from the ablation zone (including the seasonal snow and bare-ice zones). These regions are shown as progressively darker to illustrate the decreasing albedo. This figure is not to scale, and the hydrological processes might not occur concurrently and might vary across the ice sheet in response to different climates. Ice sheets contain many complex features, which strongly affect the characteristics of firn.

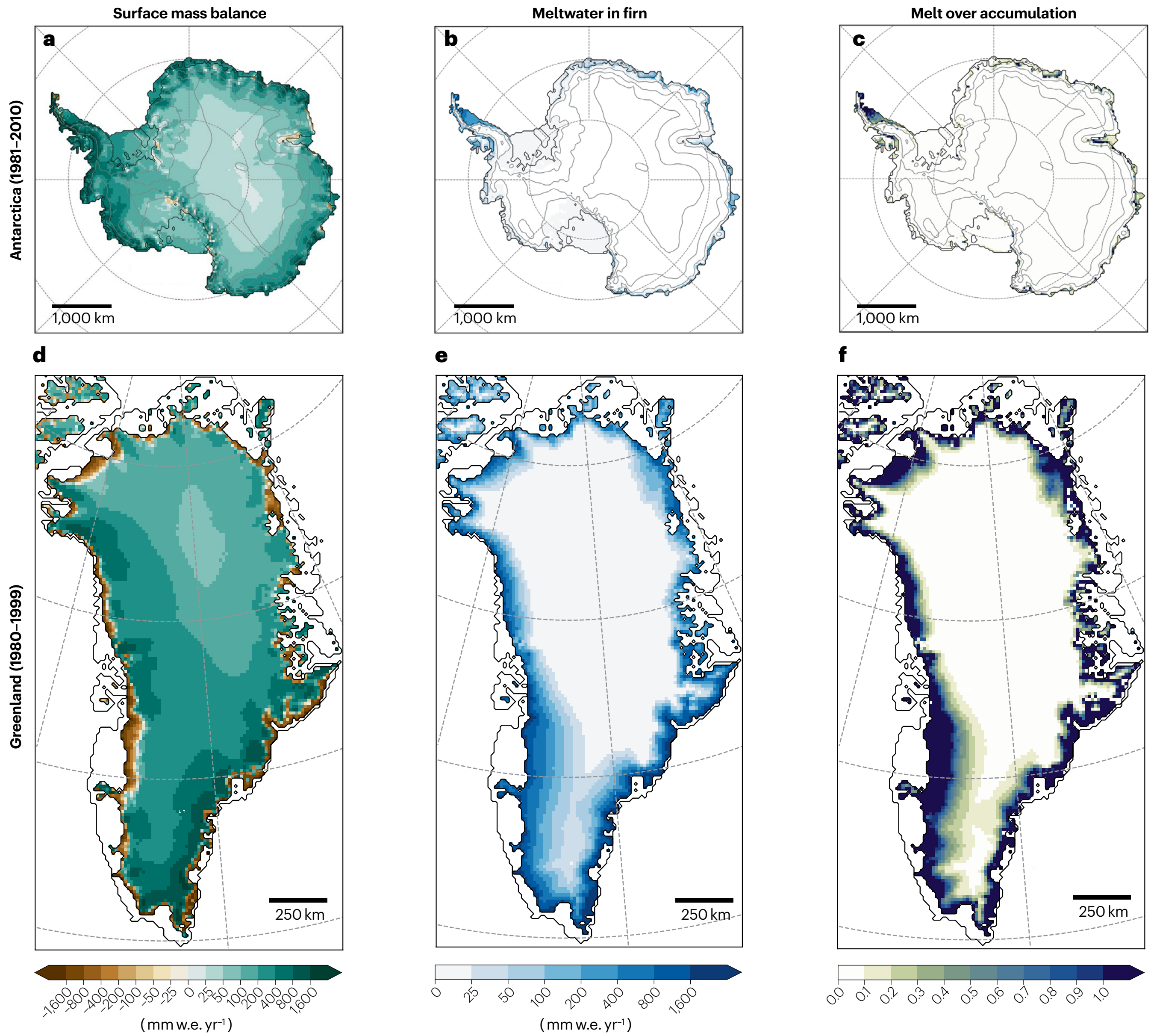


**Fig. 2 | Current metrics for firn on the Antarctic and Greenland ice sheets.** **a**, Modelled local surface mass balance (SMB, the local balance of surface mass fluxes including precipitation, sublimation, evaporation, erosion and runoff) for the Antarctic ice sheet. The values are calculated as a yearly mean from 1981–2010, derived from MAR v3.11 (ref. 260) forced with CESM2. w.e., water equivalent. **b**, As in **a**, but for annual surface melt (meltwater in firn or on bare ice). **c**, As in **a**, but for melt over accumulation (MOA, if this value exceeds 0.7, meltwater starts to pond or run off). **d**–**f**, As in **a**–**c**, but for the Greenland ice sheet, with values derived as a yearly mean from 1980–1999 from MAR v3.12 (ref. 293) forced with CESM2. The reference periods for each ice sheet are characterized by a relatively stable SMB. Currently, regions with negative local SMB, meltwater in firn and MOA > 0.7 extend to higher elevations in Greenland than in Antarctica.

## Firn properties

Firn comprises a matrix of ice grains and air. It can be characterized by properties ranging from the microscale (grain) to the macroscale (bulk sample). The matrix forms after individual precipitating or drifting snow particles accumulate at the snow surface and undergo sintering following vapour diffusion along the grain boundaries[62]. Microscale firn properties relate to the structure and geometry of the ice matrix. Examples of common microstructural properties are grain size and shape, specific surface area, sphericity, coordination number and *c*-axis orientation[63–66]. Initial microstructural properties of snow are determined by atmospheric conditions[67,68]. Once buried, the microstructure evolves owing to snow grain metamorphism driven by vapour pressure dependencies on temperature and grain size that alter grain properties over time[69].

At the macroscale, the dry density $\rho_d$ is defined by the mass of solid ice in the matrix relative to the volume and is closely related to the porosity $\phi = 1 - \rho_d/\rho_{ice}$, where $\rho_{ice}$ is the ice density. Porosity affects fluid, vapour and air transport and water storage in the firn, and it sets the upper bound for the volume of meltwater that can be refrozen or stored in aquifers. FAC is defined as the integrated porosity over the thickness of the firn. The wet firn density includes the masses of both the liquid water and solid ice in the firn matrix.

Firn density generally increases with depth (Fig. 3). The density of fresh surface snow is determined by atmospheric conditions, particularly temperature and wind speed. With increasing wind speed and temperature, as well as with very low temperatures, fresh snow density tends to increase[68,70]. After initial snowfall, drifting snow, compaction and meltwater refreezing can increase the surface density to around 280–420 kg m$^{-3}$. Subsequent densification of dry snow is entirely due to compaction and is primarily driven by overburden pressure from the mass of the overlying snow[71]. Densification occurs most rapidly up to a density of ~550 kg m$^{-3}$, and is driven by settling (that is, the physical packing and rounding of snow grains). Between densities of ~550 kg m$^{-3}$ and ~830 kg m$^{-3}$, the dominant processes are recrystallization and deformation, which include sintering as stresses between grains decrease the pressure melting temperature along grain contacts[72], and deformation along the basal planes of ice crystals[63]. Finally, beyond the pore close-off density of ~830 kg m$^{-3}$, the ice matrix becomes impermeable to fluid movement and is no longer considered firn, but glacial ice. Densification is then achieved by the compression of closed-off pore space, driven by deformation of the ice and the disequilibrium between the hydrostatic pressure in the ice and the air pressure in the bubbles.

In wet firn, densification can occur through compaction and local mass influx. Compaction in wet firn is faster than in dry firn because melting makes grains more rounded[41,69], and meltwater lubricates the grains making packing more efficient[73,74] (Fig. 3). Additionally, water that fills the pore space can refreeze, which further increases the dry density. Wetting also influences the grain size of firn, whereby the grain size increases most rapidly on first wetting and in water-saturated firn, where smaller grains melt first while larger grains grow[69]. At low liquid water content, grains congregate in large, tightly packed grain clusters[69].

Microstructural properties affect the optical[75] and thermal properties of the firn, which affect the exchange of energy with the environment. Albedo is reduced with increasing grain size and ranges from 0.35–0.5 for clean, bare ice to 0.9 for clean, dry snow[75]. Impurities and snow wetness can further decrease albedo, to as low as ~0.2 for dirty ice. Meanwhile, the thermal conductivity depends strongly on density. Firn air in the pore space reduces the thermal conductivity[76]; low-density firn (~100 kg m$^{-3}$) has a thermal conductivity of less than 0.1 W m$^{-1}$ K$^{-1}$. Firn microstructure is a key control for thermal conductivity at low densities because the bonds between grains act as the conduits for heat conduction[76]. As the firn density increases, the thermal conductivity also increases until it reaches the ice conductivity of 2 W m$^{-1}$ K$^{-1}$ as the firn becomes glacial ice.

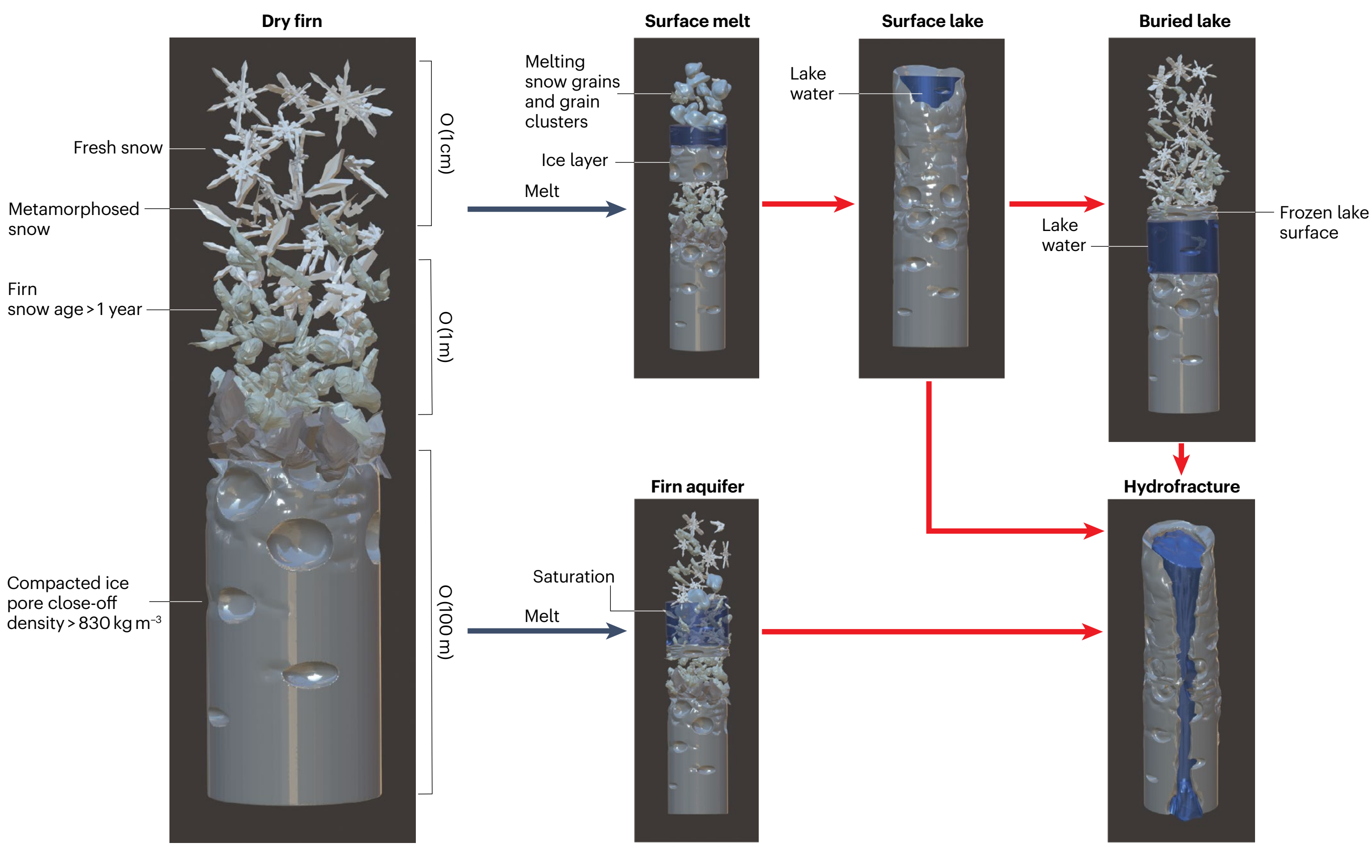


**Fig. 3 | Effects of meltwater on firn structure.** Schematic representation of a dry firn column undergoing melt, producing surface hydrology features that include meltwater, potentially leading to hydrofracture. Depth scales for the upper snow layer, firn layer and compacted ice are indicated. The interaction between meltwater, firn and compressed ice can affect the retention of mass in the ice sheet through numerous pathways.

Temperature strongly influences firn evolution. For example, increasing temperatures drive an exponential increase in the compaction rate[77–79]. Additionally, the evolution of many microstructural properties depends on the temperature and temperature gradient[80,81]. For example, grain growth rates increase with temperature[65]. Grain size also increases with the age of the firn and is approximately linear with depth[82,83]. Increased grain size decreases the densification rate[77].

Although the macroscale properties firn density and porosity quantify the total pore space available for fluid transport through the firn column, microscale properties provide an additional control on the ease of fluid flow through firn (permeability) and influence the effective diffusivity of gases[84–86]. Differences in the microstructure of firn originating from different depositional events can be preserved in adjacent firn layers, even when the density is the same[85]. Additionally, the near-surface microstructure and density[87] as well as the surface roughness[88] determine the exchange of air between the atmosphere and the near-surface firn layers.

### Firn hydrology

Liquid water, originating from surface melt or rain, strongly interacts with the firn structure as it flows through the pore space (Fig. 3). Current models suggest that Greenland surface melt is of similar magnitude to the total precipitation but only about 50% of the generated surface meltwater runs off into the ocean[89], with the remaining 50% being retained in the firn by capillary forces or refreezing. However, since roughly 2000, meltwater runoff into the ocean has become the primary source of mass loss for the entire Greenland ice sheet[90]. In Antarctica, sublimation is currently the dominant surface ablation process, with the annual surface melt volume (40–100 Gt yr$^{-1}$) estimated to be around half of the annual sublimation (110–160 Gt yr$^{-1}$), and in turn, runoff is at most a few per cent of the surface melt flux (0–2 Gt yr$^{-1}$; refs. 9,91) because almost all of the surface meltwater is retained in the firn[2]. Surface melt is largely absent over the interior of the East Antarctic Ice Sheet[36], and modelling shows that since the early 1980s, SMB has generally been positive[2,9,91], resulting in a stable firn thickness. Understanding the interactions between water flow and the ice matrix is crucial for determining the fate of meltwater in the ice sheet.

The physical model considered in firn hydrology is that of a viscous liquid flowing through a variably saturated porous medium in which the pore fluid and matrix can change phase. Initially, water invades the air-filled pore space between ice grains, driven by surface tension gradients and gravity[92]. The rate of percolation, depth of infiltration and spatial patterns of subsurface saturation are controlled by the permeability of the firn — that is, the balance between viscous forces and capillary action — and by the thermal state[93–95]. The permeability of firn is heterogeneous, owing to centimetre-scale microstructure anisotropy[64], causing heterogeneous infiltration. For example, fingering instabilities develop in alpine snow, when water ponds at capillary barriers or the leading edge of the wetting front[96–98], forming preferential flow pathways. This preferential flow seems to be the dominant mode of flow in subfreezing, unsaturated firn[99–101] and enables deeper percolation than would be expected for homogenous percolation.

Water initially enters firn that is below the freezing point, causing the percolating water to refreeze. Therefore, firn temperature controls and limits the depth of infiltration[102,103] and the extent of lateral migration[100]. Refreezing alters the macroscopic permeability of the firn and reduces its water storage capacity by filling some pore space with refrozen ice. Refreezing also releases latent heat that warms the surrounding firn and reduces its capacity to refreeze subsequent infiltration[104].

Refreezing produces a strong feedback mechanism between water infiltration and the physical, hydraulic and thermal properties of firn. These complex interactions lead to very different firn hydrological systems in different parts of the ice sheet that can affect SMB, as well as ice dynamics, by modulating water input to the subglacial system. In the percolation zone, meltwater refreezes locally within the firn to form embedded ice layers, lenses, and pipes[73,105]; therefore, meltwater is retained locally and does not contribute to ice-sheet mass loss[106]. However, there is a gradient in refrozen ice content across the percolation zone, with these features occupying a large proportion of available pore space at low elevations where melt is high and snowfall is low[46]. Near the equilibrium line, meltwater input can meet or exceed the volume of available firn pore space, leading to the formation of features such as ice slabs[45] and firn aquifers[107,108] that contribute to the export of meltwater from the firn to other parts of the hydrological system (Fig. 1).

In high-melt, low-accumulation areas, percolated meltwater can refreeze in ice slabs inside the firn. These multimetre-thick continuous layers of refrozen ice form just below the firn surface (Fig. 1b) and are sufficiently impermeable to block vertical percolation[46,47]. Subsequent surface melt can then form supraglacial streams that run off to lower elevations[47,109], drain into the relict firn layer through surface crevasses[110,111] or collect in supraglacial lakes that can later drain to the ice-sheet bed through hydrofracture[112] (Fig. 3, bottom right). If there is sufficient insulating accumulation, buried lakes can also form and impound water for multiple years[39,113]. In Greenland, ice slabs are currently estimated to cover 60,400–73,500 km$^2$ (ref. 14) (Fig. 4b) and to have expanded the ice-sheet runoff zone by ~26% since 2001 (ref. 45), leading to enhanced surface mass loss[46]. Extensive ice slabs are not yet common in Antarctica, although similar depletion of firn pore space[114] and subsequent lake formation and drainage processes[109,110] occur in high-melt areas on ice shelves that experience repeated local inundation of the firn. The expansion of surface ponding in these regions can contribute to ice-shelf hydrofracture (Fig. 3).

In high-melt, high-accumulation regions, new snow can insulate wet firn from cold surface temperatures[115] leading to the formation of nearly saturated subsurface aquifers that persist over the winter (Fig. 3, bottom centre). In areas with surface elevation gradients, these aquifers can efficiently transport meltwater from high to low elevations[15,116,117], but it is generally considered that they delay the runoff of meltwater on the short term[117]. In Greenland, firn aquifers cover at least 21,900 km$^2$ (ref. 107) (Fig. 4b), with the largest aquifer at Helheim Glacier storing between 2.2 and 4.8 Gt of water[16,116,118]. However, it is likely that this water drains to the ice-sheet bed through hydrofracture at the aquifer boundaries[18], leading to year-round water input to the subglacial system that can dampen seasonal ice-velocity fluctuations[119]. Firn aquifers have also been identified on some ice shelves in the Antarctic Peninsula (Fig. 4a), where they contribute to hydrofracture-driven damage and the breakup of ice shelves[109,120].

All of these firn structure changes caused by water percolation and refreezing can affect firn hydrology for decades[46]. It is this combination of strongly coupled nonlinear processes and the long memory that makes it so challenging to model water percolation.

## Firn observations

Observations are used to design, constrain and tune firn models and have been indispensable in establishing a continent-scale picture of

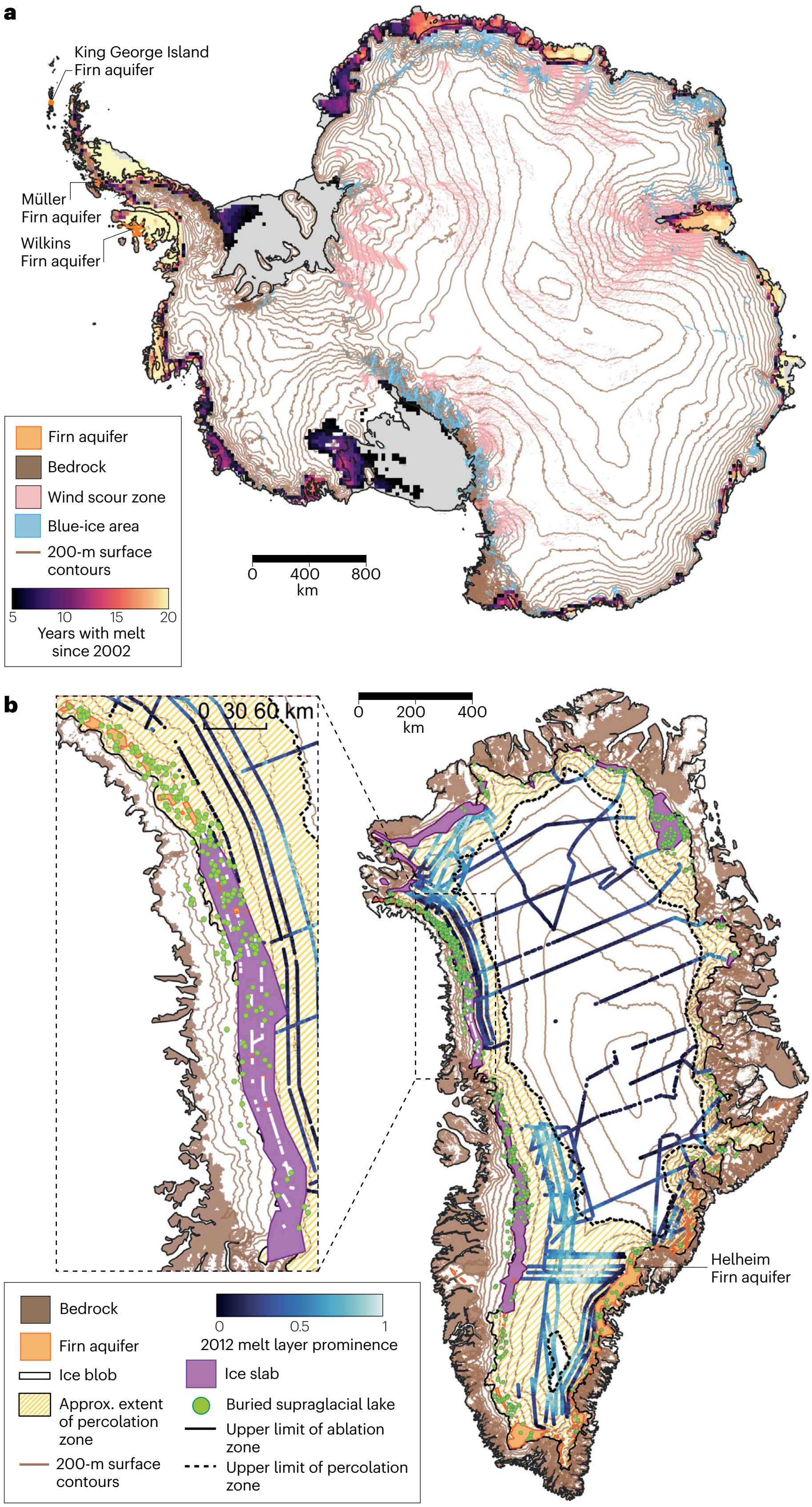


**Fig. 4 | Firn facies and features on the polar ice sheets. a**, Surface topography of Antarctica from BEDMAP2 (ref. 294) and firn features, including regions exhibiting melt (purple–yellow shading; where at least 5 years are detected by passive microwave instruments[295] between 2000 and 2020); known firn aquifers[120,194] (orange); wind scour zones[296] (light pink); and blue-ice area[297] (blue). **b**, Surface topography of Greenland from BedMachine Greenland[298] and firn features, including a proxy for the extent of the percolation zone (yellow hatching; any region above the upper limit of the summer bare-ice zone[299] where passive microwave instruments detected at least 5 mm of water equivalent (w.e). melt over the melt season[300] for at least 5 years during 2007–2015); ice slabs[45] (purple); firn aquifers[107] (orange); buried supraglacial lakes[285] (green dots; as mapped in the summer of 2019); and the 2012 melt layer prominence metric[258] (blue shades; the horizontal continuity and density of a subsurface ice layer formed during the 2012 extreme melt season measured by airborne surveys, where a value of 1 or more corresponds to a horizontally continuous, solid ice layer[258]). The solid and dashed black lines indicate the upper limits of the ablation and percolation zones, respectively. Inset: enhanced details of the multiple hydrological features in northwest Greenland with ice blobs[111] shown in white. These spatial variations in firn structure and hydrology reflect the history of firn–atmosphere interactions in each region and modulate the local surface mass balance.

the prevalence of firn facies and features (Fig. 4). This section discusses the strengths and weaknesses of the various observational techniques.

### Surface mass balance and firn structure

The evolution and properties of a firn layer such as annual accumulation, thickness and FAC can be monitored using various techniques. First, atmospheric conditions that determine firn appearance are monitored continuously using automatic weather stations, in Greenland[121,122] and Antarctica[123]. Accumulation can be derived from measurements from acoustic or laser height sensors, augmented with density information from in situ snow profiles[124], which sample the upper few metres of the firn, or from firn models[125]. Firn density is determined by measuring the volume and mass of a sample. Snow temperatures and stratigraphy observations (grain size and shape) are also often made in a snow pit to understand the evolution and metamorphism of the snowpack (Fig. 3). Shallow firn cores and deep firn cores, of which some reach pore-close-off depth, can be drilled to obtain a longer record of firn properties. They have been used to generate local and regional reconstructions of FAC[126,127] and local SMB[29,128] spanning several centuries. However, snow pits and firn cores are time-consuming to obtain and often inadequately capture spatial variability.

Non-destructive measurement approaches, using wave-based geophysical techniques such as seismics or radar, have been developed to capture firn properties on large spatial scales (Fig. 5). Ground-based radar systems, which are often mounted on a sled and towed over the surface by snowmobiles, can map internal reflection horizons with vertical resolution of tens of centimetres[129]. These internal reflections arise because the firn permittivity of electromagnetic waves depends on density. These measurements can reveal the spatial and temporal variability of local SMB across ice sheets from interannual to decadal timescales and over many hundreds of kilometres[130–132]. Data from repeated radar surveys can be used to

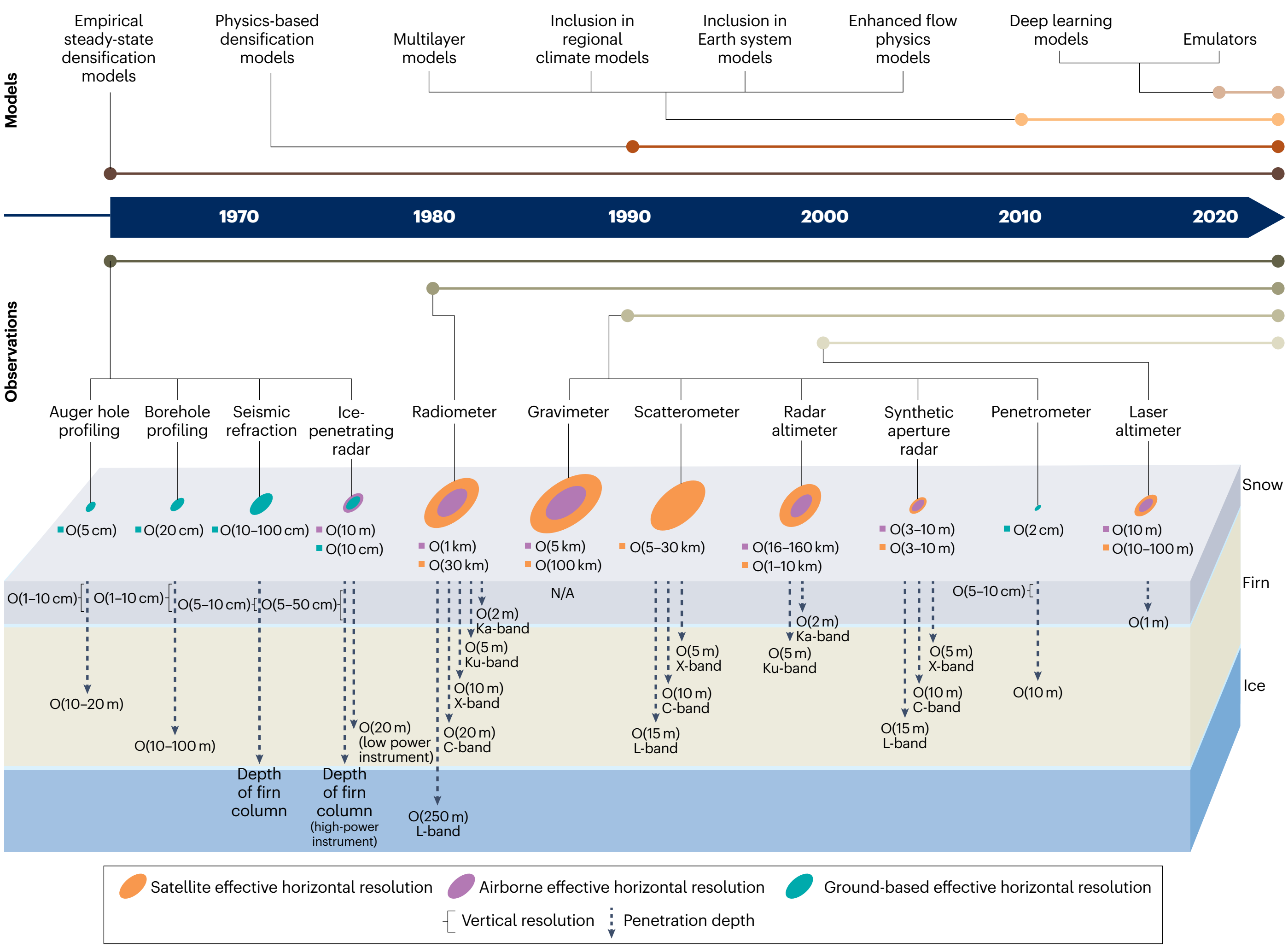


**Fig. 5 | Modelling and observational techniques.** Timeline of the development of firn models applied to ice sheets (top) and observations, including satellite, airborne and ground-based techniques (bottom). The orders of magnitude for the effective horizontal resolution (pink, orange and green), vertical resolution (in black square brackets) and penetration depth (grey dashed arrow, for different frequencies where appropriate: L-band, 1–2 GHz; C-band, 4–8 GHz; X-band, 8–12 GHz; Ku-band, 12–18 GHz; Ka-band, 26.5–40 GHz) with approximate depths of snow, firn and ice shown for perspective. These advances in both modelling and observations have made it possible to examine firn in finer detail.

quantify firn compaction[133,134]. With wide-angle observations, vertical density profiles can be derived from the travel time of radar waves[129,135] using empirical relations between density and velocity[136,137]. Mobile receiver arrays could be used to efficiently map lateral variability in firn density[132], removing the need for labour-intensive repositioning of individual antennas.

Active and passive seismic surveys make use of the dependence of seismic velocity on the elastic properties (for example density) of firn, from which density profiles and firn thickness can be derived. Passive sensors, which measure with long time periods (months to years) and low spatial resolution (tens to hundreds of kilometres), record ambient noise. In contrast, active sensors, which perform instantaneous measurements with high spatial resolution, record actively triggered seismic waves — for example using small explosives or a hammer and metal plate. Seismic methods are used to observe variations in firn thickness over regions on a kilometre scale[138–140]. A seismically observed velocity–depth profile can be translated empirically into a density–depth profile[141]. The full elastic waveform can be used to measure density heterogeneities such as ice slabs[142]. Further, the different seismic velocities of compressional and shear waves can be used to derive mechanical properties of firn that govern firn compaction and crevasse formation[143,144]. The splitting of shear waves indicates anisotropic crystal orientation, which promotes ice flow by shearing[145,146], and such anisotropy can already emerge in the firn before it is compressed into ice[143,147]. A notable implication from these observations is that ice flow can be influenced by firn densification even before the ice has formed.

Although ground-based remote-sensing techniques can achieve a larger spatial coverage than point measurements from, for example, weather stations, snow pits and firn cores, their spatial and temporal coverage is still determined by logistical access. These limitations can be overcome by air- and spaceborne instruments, which can be operated on the ice-sheet scale. Such instruments offer large spatial and temporal coverage and have a high revisit frequency; however, these advantages come at the cost of reduced spatiotemporal resolution in both the horizontal and vertical directions.

Lidar, or laser scanning instruments, on board aircraft (such as NASA Operation IceBridge, Thematic Mapper and ESA CryoVEx[148]) and satellites (NASA ICESat and ICESat-2[149,150]), use the reflection of laser light from the snow surface to accurately measure surface elevation changes. However, laser-based measurements are limited to clear-sky conditions. Radar sensors (including ESA's ERS-1/2, ENVISAT, CryoSat-2 and Sentinel-3A/B) avoid this limitation, but, in contrast to laser light, radar waves penetrate into the near-surface firn layers[151–153], as a function of frequency. Generally, aeroplane-based observations can obtain higher spatial resolution and receive signals from deeper down in the firn (100–200 m) than spaceborne sensors (down to 10 m). Physics-based firn models are often needed to extract the observed surface elevation change from radar measurements, owing to complications arising from changes in radar wave propagation and ice dynamics[150,154–157]. Backscatter modelling enables the use of remote sensing to observe surface density variability[158] and compaction rates[159,160].

Advances in radar altimetry processing have enabled direct observations of near-surface firn densities and roughness from the observed return power of radar reflections[161]. It is expected that these observations of near-surface density will soon make it possible to directly convert the observed volume change derived from surface height change into mass change without the use of firn models[161]. However, despite the many advantages of remote sensing, in situ observations often remain crucial as a ground-truth for the development of retrieval algorithms and for evaluating spatial heterogeneity.

### Observing the fate of meltwater

To assess sea-level rise in a changing climate, it is crucial to follow the meltwater produced at the surface of the ice sheet to uncover whether it is locally stored, routed towards other parts of the ice sheet, or running off into the ocean. Meltwater formation can be inferred when the snow surface temperature measured by automatic weather stations[162] reaches melting point. The presence of meltwater at the surface can also be detected visually in snow pits, or quantified by dielectric measurement techniques, which use an empirical relationship between the dielectric constant of snow and its porosity and/or water content[163–166]. Alternatively, the presence of surface meltwater can be derived from remotely sensed visual imagery, or from air- and spaceborne active sensors, such as synthetic aperture radars and microwave scatterometers[167,168]. These sensors have small penetration depths of only a few metres, making them ideal to monitor the near-surface properties of the firn layer.

To determine what happens to the produced meltwater, water flow by percolation can be made visible by tracing coloured dye that is sprayed onto the ice-sheet surface before the melt season. When the melt season is over, the dye detected in snow pits or shallow firn cores reveals percolation and ice-layer formation, which can both occur at depths up to several metres[169]. Rates of vertical and lateral meltwater flow through snowpacks can also be monitored using tracers in real time, for example using a stable isotopic tracer solution[170]. Piezometers, portable lysimeters, salt-dilution and tracer experiments have been used to measure hydraulic conductivities of firn areas of the Greenland ice sheet that contribute to runoff[171]. Combined with slug tests, these methods have also been used to determine the hydraulic conductivity and flow rates in firn aquifers[120,172].

Electrical self-potential methods[173,174] are promising approaches for measuring meltwater because they are cheap, and directly measure lateral and vertical liquid water flow, with minimal invasive impact. Horizontal and vertical firn permeability can be estimated over a bulk volume of the order of one to several cubic metres, using pneumatic testing using bore holes[175]. Additionally, radar techniques can detect the water content in firn because the dielectric permittivity and the scattering mechanism depends on the water content and the shape of water inclusions[176,177]. This technique has even been used in setups with buried radars that look upwards to detect meltwater percolation[101]. Although seismic and radar methods can be used to observe hydrological processes[178], they are not effective for quantifying the hydraulic properties of firn. Destructive testing is generally required to measure these properties, as discussed above. Developments have been made in the use of magnetic resonance sounding to non-destructively obtain liquid water volumes in the firn[179].

Percolating meltwater processes can also be inferred from observations of the resulting changes in firn structure. Vertically installed thermistor strings can detect heating owing to the release of latent heat on refreezing[100]. Alternatively, refreezing can be studied by observing the changes in microstructure and density that it induces, such as the formation of melt grain clusters and ice layers. Liquid water and firn aquifers can be locally detected directly from the presence of water when extracting a firn core[108]. Remote sensing combined with backscatter modelling enables the observation of firn aquifers[107,180] and ice layers[45] on continental scales. The strong dependence of microwave penetration depth on frequency also enables remotely sensed observations of internal ice-sheet temperature profiles[181] and water content[182].

### Records of the past

Firn cores provide records of the past because they contain layers associated with past accumulation and melt events. Layers in the stratigraphy can be identified manually, with infrared imaging, or with computer vision[183]. Dry firn cores can also be dated by studying the annual layering created by the seasonal deposition of stable water isotopes, major ion chemistry or photochemical species (such as hydrogen peroxide). Markers of volcanic fallouts and atmospheric nuclear testing[184,185] provide absolute timing constraints. The distance between seasonal markers – the annual layer thickness – can be converted to metres of water equivalent by multiplying it with measured firn density. Plastic deformation results in ice layers becoming thinner and expanding horizontally as they become buried deeper. Ice-flow models can be used to correct for this process, as a function of depth[186].

Firn-core density profiles can be established with very fine vertical resolution using sophisticated instruments that measure the scattering and absorption of γ-ray, X-ray or neutron radiation[187–189]. Other methods that yield accurate, high-resolution density observations are dielectric profiling, ice-core scanners and borehole optical televiewing[114,190]. This high resolution is needed to determine the annual and intra-annual variability in accumulation and firn properties, especially in low-accumulation areas. X-ray measurements have also been used to obtain three-dimensional images of the firn and ice microstructure, for example to follow the pore close-off process[191].

Melt events can be reconstructed by studying the ice layers that form on refreezing[192], which are even detectable at the submillimetre scales using digital line-scanning[184]. Although single firn cores can be used to identify refrozen ice layers[46,193], multiple cores from across a large area can reveal detailed variability in refrozen firn grain structures to support theories of firn aquifer formation within an ice shelf[194]. However, for large-scale (kilometre-scale) measurements, refrozen ice layers are often tracked using ground-penetrating radar[161] or seismic[138–140] techniques. Whether and how melt-affected cores can be dated and used for climate reconstruction is currently under discussion[159].

In the accumulation zone, firn ultimately compacts into ice. Therefore, ice cores provide important clues into the characteristics of past firn[195]. For example, air enclosed in the ice provides three direct observational constraints on past firn conditions: the $^{15}N/^{14}N$ stable isotope ratio ($\delta^{15}N$) of $N_2$; the oxygen to nitrogen ratio ($\delta O_2/N_2$); and the gas-age–ice-age difference (Δage) that is, the age difference between the ice and the air trapped in closed bubbles inside the ice, with the former being older.

The $\delta^{15}N$-$N_2$ ratio is enriched under gravity until the lock-in depth is reached. Thus, the $\delta^{15}N$ in the trapped air bubbles can be used to estimate past pore close-off depths[196]. The $\delta^{15}N$ value is also affected by thermal fractionation in the presence of temperature gradients, and it can be challenging to disentangle the gravitational and thermal contributions. To do so, $\delta^{15}N$ records can be combined with measurements of the $^{40}Ar/^{36}Ar$ ratio ($\delta^{40}Ar$) to provide estimates of the temperature gradients because argon and nitrogen experience the same degree of gravitational enrichment per unit mass difference, but have a different sensitivity for thermal fractionation. The combined $\delta^{15}N$ and $\delta^{40}Ar$ data can thus be used to reconstruct the magnitude of abrupt climate shifts at the surface[197].

The $\delta O_2/N_2$ ratio of air trapped in ice cores suggests that both summer insolation and temperature gradients affect firn microstructure[198]. The $\delta O_2/N_2$ in firn air bubbles is lower than that of the atmosphere, because the relatively small-diameter $O_2$ molecules can leak out of newly formed air bubbles near the pore close-off depth[199,200]. This oxygen deficit is not constant through time, but follows summer peak insolation changes driven by variations in the Earth's orbit on timescales of tens of thousands of years[200]. Although the details are poorly understood, the mechanism linking insolation to pore close-off fractionation must involve changes to the microstructure of the firn itself[201,202]. The apparent detection of abrupt, millennial-scale climate change in Greenland in the $\delta O_2/N_2$ record suggests that firn temperature gradients could affect the evolution of the firn microstructure[198].

Owing to the continuous air exchange that can occur in firn, the gas at the pore close-off depth is younger than the surrounding ice matrix, resulting in a Δage that ranges from tens to thousands of years[195]. This Δage can be determined empirically with 20% uncertainty or less, using methane ($CH_4$) records to date the gas bubbles[203] combined with volcanic tie points to date the ice strata. These Δage measurements provide an estimate of the time taken for snow to transform into ice. Because this transition depends on temperature, the changes in Δage throughout an ice core can be used as a proxy for past surface temperature[204].

The largest changes in firn characteristics derived from the ice-core record are seen across the Ice Age cycles. Based on borehole-derived estimates, Last Glacial Maximum (LGM) temperatures in Greenland were around 20 °C colder than at present, whereas temperatures in Antarctica were 5–11 °C colder[205–207]. LGM SMB was around half its present-day value or less for both ice sheets. Additionally, Δage was around five times as large in Greenland[208] and around twice as large in Antarctica as at present[205], confirming that firn densification rates were strongly reduced during glacial periods. The changes in LGM firn thickness are more complex, because they represent a balance between the reduced temperature, which thickens the firn, and the reduced accumulation, which thins the firn layer. In Greenland and West Antarctica, the $\delta^{15}N$ data show that the LGM firn layer was thicker than at present, suggesting that the temperature effect dominates. In East Antarctica, the LGM firn layer was thinner than at present, suggesting the dominance of the accumulation effect[204,209].

## Firn modelling

The modelling of firn has advanced concurrently with enhanced observational capabilities. Although models vary in complexity, formulation and numerical implementation, contemporary firn models generally contain a description of densification, thermodynamics and meltwater percolation, and are forced by atmospheric or ice-core observations, reanalyses or climate model output. These models have varying purposes, including testing physical understanding of firn processes; interpreting observations, including ice cores; interpreting remote-sensing data for example data from repeat satellite altimetery; providing a surface boundary for the atmosphere over ice sheets in climate models; and assessing future ice-sheet mass balance. Firn models mostly have a similar structure, with specific process representations for dry and wet firn, as now discussed.

### General modelling concepts

Firn modelling has undergone considerable development since efforts began in the 1950s (Fig. 5). The earliest firn models provided depth–density profiles using empirical densification laws. Later, empirical formulations were increasingly replaced by physics-based ones, for example for compaction and liquid water flow. To resolve the vertical variability in firn properties, its temperature and its liquid water content, contemporary firn models use multiple layers[210], using a combination of differential equations and parameterizations to simulate firn evolution.

Some firn models are forced by mass and energy fluxes from an atmospheric model, whereas others solve the surface energy and mass balances based on meteorological parameters. Because interactions between the firn layer and the atmosphere are two-way and complex, there is an ongoing trend to improve the descriptions of firn used in climate models and Earth System Models (ESM), or even replace these descriptions with existing complex firn models.

## Modelling dry firn densification

A complete firn model includes equations that describe the conservation of mass, energy and momentum, and constitutive equations describing the material properties. For dry firn, these are often reduced to an equation for temperature evolution, and one or more equations describing densification[211,212]. Initially, the form of these densification equations was derived from the hypothesis that the proportional change of porosity is linearly related to the change in overburden stress (Robin's hypothesis[136]). The model parameters were determined empirically using density data from firn cores, on the assumption that, in a stable climate, the depth–density relation is invariant with time (Sorge's law[213]).

The success of these empirical densification formulations (such as the Herron–Langway model[71]) is remarkable, yet they have several limitations. First, they are not strictly rooted in physical first principles — for example, the conservation equations are rarely incorporated explicitly[210]; second, they neglect various physical processes, such as grain size evolution, and assume an abrupt transition between different densification regimes; third, their capacity to model transient behaviour is uncorroborated[210,214]; and last, they cannot be assumed to be accurate outside their calibration range. To overcome these limitations, two main classes of dry firn models have emerged: first, models on large spatial scales with high temporal resolution, which can be used for interpreting altimetric data, for example[77,159,215]; second, models that focus on fixed positions over long timescales for interpreting the palaeoclimate information stored in ice cores[216,217]. The two model groups have substantial overlap and are moving towards a more process-based, semi-empirical description of densification.

The densification of firn is mainly driven by pressure sintering processes, such as grain boundary sliding, dislocation creep and diffusion creep[63,72,218]. The importance of each of these processes varies throughout the firn column, leading to different densification regimes. The processes can guide process-based parameterizations on the macroscale[77,219] and microscale[220,221]. However, these parameterizations do not generally give more accurate results than purely empirical parameterizations, possibly because the densification processes in different regimes are not strictly separated[222–224] and the transition between them should be modelled gradually[225]. Additionally, the parameterizations should be calibrated using time-dependent rather than steady-state data[210].

Dry firn models have continued to be developed. For example, the representation of microstructure and its effect on densification has been improved by including grain connectivity[217,226,227], size[77,82,214] and impurity concentration[223,227,228]. Additionally, the ice dynamical effects of horizontal divergence[229,230] and strain softening[231] have been incorporated as extensions to one-dimensional densification models or can be represented by three-dimensional full-Stokes flow models that include a constitutive equation for compressible, porous firn[232].

The understanding of firn processes has substantially improved since the 1950s, which is demonstrated by the multitude of densification equations and adaptations that now exists. Many of these are implemented as options in the common modular framework of the Community Firn Model[212]. However, the different approaches are not always compatible, and a combined calibration will be needed before present knowledge can culminate in a generally applicable firn model.

## Modelling wet firn and firn hydrology

Modelling approaches for wet firn diverge more than those for dry firn[233], owing to the various formulations for meltwater infiltration[233] and poor constraints on important model parameters[5,233]. Model complexity and numerical instability are key concerns when considering refreezing, impermeable layer formation, meltwater retention and flow within water-saturated firn layers. The balance between the physical complexity represented by the models and computational efficiency is considered in the wet firn models discussed here, including bucket models, models based on Darcy's law, models based on the Richards equation, preferential flow models and, finally, multidimensional firn models.

Water percolation in firn models is generally based on the capillarity of firn, whereby the amount of water that firn can hold with capillary forces is related to its density and grain size[66,215,234]. Incorporating this concept in models is essential to capture the meltwater storage in firn. In bucket models, water exceeding the capillary capacity can percolate downward instantaneously. Percolation stops when the water reaches a layer with a temperature below the melting point with sufficient pore space to refreeze, or when it reaches an impermeable layer. Water leaving the bottom of the simulated firn column is considered runoff. An alternative group of models use Darcy's law, which describes the flow of a fluid through porous media. These Darcy-type models solve the balance between capillary suction and gravity[93,95,235], which generally provides a better simulation than bucket models of the downward percolation speed and the inhomogeneous water distributions caused by microstructural transitions in firn. Reproducing these processes is important to enable an accurate description of the formation of ice layers[236]. Models solving the Richards equation, a formulation of Darcy's law for unsaturated flow, often provide better agreement with observations than bucket-type models[234], although mainly at shorter timescales and with additional computational cost.

Neither bucket nor Darcy-type models account for water flow in preferential paths[237]. Efforts have been made to parameterize this process either using depth-dependent parameterizations[238] or by separating percolation into two regimes[236]. Preferential flow can also be simulated using centimetre-scale two-dimensional models, because it can be guided by spatial heterogeneity in firn structure[99,239]. Even though it is not currently feasible to use such models on the ice-sheet scale, they can still advance the understanding of the role and importance of preferential flow in forming hydrological features and generating runoff.

Additionally, bucket and Darcy-type models cannot produce a satisfactory solution for the interaction of meltwater with ice lenses and ice slabs, which prevents them from assessing the extent to which these features increase runoff from the ice sheet. Model representations of ice slabs and ice lenses vary widely. Some models ignore them, assuming that some penetration path always exists at the kilometre scale at which the model is applied[215,240]. Other models assume that there is no water percolation, and that any rain or meltwater produced immediately saturates or is treated as runoff[233]. Some models allow percolation and ice lens or slab formation but tend to over-predict their formation[233]. Multidimensional firn models are required to simulate lateral water flow in firn (for example in aquifers[241]) and to improve the simulation of the amount and timing of runoff over impermeable ice slabs or the firn–ice interface. However, the computational cost of such models is still prohibitive for large-scale applications, which makes it challenging to use these models to assess future firn hydrology.

### Modelling chemical tracer transport

Modelling the transport of atmospheric trace gases within the firn supports the interpretation of records of past environmental change. For these applications, the pore space is divided into open and closed porosity, with the former reflecting pores that remain interconnected with each other and the overlying atmosphere, and the latter reflecting pore clusters that are effectively isolated or closed off. The open pores aid the movement and mixing of atmospheric gases. Gas transport is dominated by molecular diffusion, but downward advection, near-surface convection, and dispersion also have a role[195,242]. One-dimensional numerical models of firn air transport can skilfully simulate the distribution of atmospheric tracers in dry firn[243,244]. The effective vertical diffusivity of firn is difficult to predict from first principles or measurements because of the highly irregular pore structure, and a common modelling approach is to calibrate the model using trace gases with a known atmospheric history[245–247].

The pore space also aids the diffusion of water molecules in the vapour phase[248]. This process attenuates centimetre-scale spatial variations in water stable isotope ratios, resulting in a loss of the seasonal cycle in water isotope ratios ($\delta^{18}O$ and $\delta^{2}H$) at most sites[249]. Numerical modelling of water isotope diffusion can be used to reconstruct this annual signal[248,250].

## The changing ice-sheet and ice-shelf firn

Observation and modelling techniques have made it possible to assess changes in firn characteristics caused by anthropogenic warming and evaluate potential future changes. Both these aspects are now discussed. However, it is important to note that any changes, particularly projected changes, have an associated uncertainty — thus, findings should be interpreted with caution.

### Observed changes

Observations of warming and extreme weather events over Greenland and Antarctica have made it possible to better understand the potential impact of a warmer future on firn characteristics. Since the satellite era (1979 to present), surface melt over the Antarctic ice shelves has been limited[251], but some ice shelves have experienced brief, but intense, melt events. For example, atmospheric rivers and associated foehn winds[55,252] occurred over the Larsen C ice shelf in the Antarctic Peninsula, which coincided with a multidecade period of strong atmospheric warming[253], triggering intensive melt events that resulted in firn densification and firn air depletion[254]. These mechanisms have strongly preconditioned most of the Antarctic Peninsula ice-shelf collapses that have occurred since the 1970s[255]. By contrast, relatively little change in firn thickness has been observed on the East Antarctic ice sheet[5], despite anomalous events being recorded, for which the link to climate change is uncertain. For example, in 2022, a highly anomalous heatwave occurred over East Antarctica, adding substantial precipitation. Partially because of this event, 2022 had the highest recorded Antarctic SMB since the beginning of the satellite record[256].

Over Greenland, repeated intensive melt summers have caused the inland expansion of metre-thick, low-permeability ice slabs. Since 2001, overall temperature trends in Greenland have remained unchanged, although between 1991 and 2019, coastal regions experienced summer and winter warming of approximately 1.7 °C and 4.4 °C, respectively[48]. Atmospheric warming[48,257] and changes in tropospheric circulation seem to have led to a decrease in firn permeability, particularly after the 2012 melt season[258]. This assertion is supported by a modelled expansion of the Greenland ablation area and an observed increase in the runoff area. Observations indicate that firn retention capacity (as captured by FAC) has changed in different facies of the Greenland ice sheet. Although the FAC over the dry snow zone has not changed substantially since 1953, large changes have occurred in the percolation zone; for example, the firn retention capacity reduced by 150 ± 100 Gt during 1998–2008 and 540 ± 440 Gt during 2010–2017 (ref. 127). Increased rainfall can also contribute to FAC depletion and warming of the firn through refreezing, as evidenced from a single rain event in late October 2008, that produced warming effects comparable to those of summer surface melt[259].

### Future changes

In all future climate scenarios, the atmosphere over the Greenland and Antarctic ice sheets is projected to warm to a varying degree, leading to enhanced liquid water in firn as a result of increased precipitation[19,23], a greater ratio of rainfall to snowfall[20,21], and increased surface melt[22,23].

Future changes to Antarctic and Greenlandic SMB, surface melt and MOA are anticipated (Fig. 6), albeit with uncertainty inherent to both the driving ESM and the regional climate model parameterizations and climate sensitivity. SMB over Antarctica is primarily driven by changes in snowfall, which has increased in the twentieth century at the rate of 2.5 mm decade$^{-1}$ since 1979[29] and is projected to increase substantially in the future within the dry interior[260] (Fig. 6a). In Antarctica, surface melt is currently small (70–100 Gt yr$^{-1}$) compared with SMB (~2,200 Gt yr$^{-1}$)[9] and mostly limited to the floating ice shelves that surround the continent (Fig. 2b). However, the disintegration of these ice shelves, accelerated by the formation of melt ponds after firn air depletion, could lead to increased mass loss. Surface melt rates are anticipated to increase substantially over the ice shelves in the future, from a mid-century scenario-independent doubling[261] up to an order of magnitude increase by the end of the twenty-first century for high-emissions climate scenarios[22,262]. The intermediate climate scenario projects a surface melt anomaly (Fig. 6b) corresponding to a threefold increase in ice-shelf surface melt rates by the end of the century.

As ice-shelf resilience, captured by MOA, is affected by snowfall as well as melt, the critical threshold of 0.7 can be reached both in regions where air temperature and melt are high, such as the Larsen C ice shelf, and at lower temperatures in regions with less precipitation, such as the Amery, Ross and Filchner–Ronne ice shelves (Fig. 6c). Ice shelves are more vulnerable in scenarios with greater predicted warming[263,264]: for example, the Larsen C and Amery ice shelves are expected to reach MOA = 0.7 under a medium greenhouse gas emission scenario (Shared Socioeconomic Pathway SSP2-4.5) whereas the Ross ice shelf reaches this threshold only in the high emission (SSP5-8.5) scenario (Fig. 6c).

Unlike Antarctica, most of the Greenland ice sheet terminates over land. SMB is projected to increase in the high-elevation interior, as in Antarctica, but decrease at lower elevations over a proportionally much larger area than for Antarctica, owing to increased runoff and the

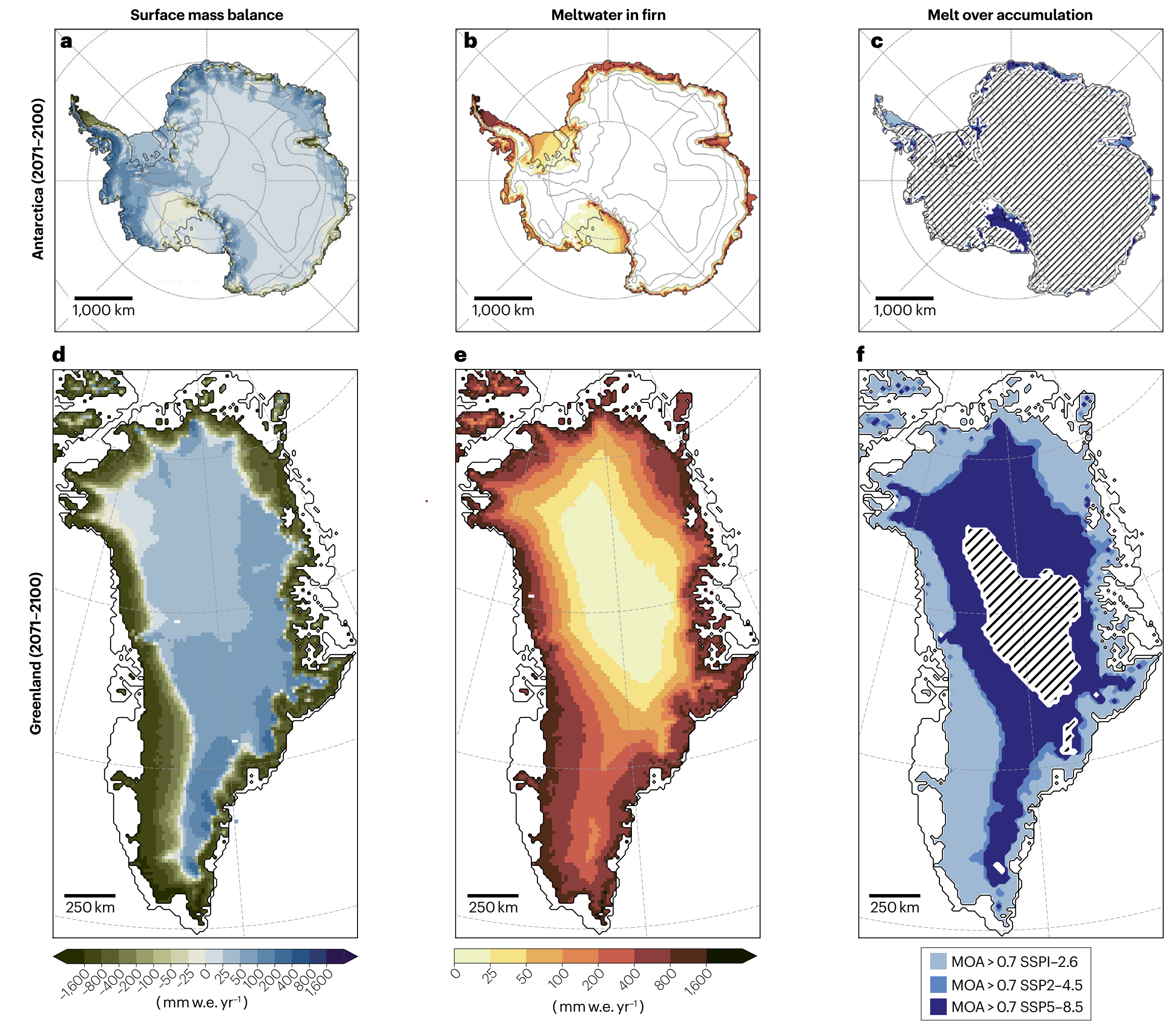


**Fig. 6 | Future metrics for firn on the Antarctic and Greenland ice sheets.** **a**, Yearly average surface mass balance (SMB, the balance of surface mass fluxes including precipitation, sublimation, evaporation, erosion and runoff) anomalies for the Antarctic ice sheet during 2071–2100 relative to 1981–2010. Anomalies are derived from MAR v3.11 (ref. 260) forced by one CESM2 ensemble member under a medium greenhouse gas emission scenario (Shared Socioeconomic Pathway SSP2-4.5). w.e., water equivalent. **b**, As in **a** but for annual surface melt (liquid water in firn or on bare ice). **c**, As in **a** but for regions where the melt over accumulation ratio (MOA) exceeds a threshold value of 0.7 (above which meltwater starts to pond or run off), under low, medium and high greenhouse gas emission scenarios (SSP1-2.6, SSP2-4.5 and SSP5-8.5, respectively). The hatched area indicates regions where MOA < 0.7 for all scenarios. **d**–**f**, As in **a**–**c** but for the Greenland ice-sheet anomalies during 2071–2100 relative to 1980–1999 derived from MAR v3.12 (ref. 293). The reference periods for each ice sheet are characterized by a relatively stable SMB. Future warming is projected to cause the inland expansion of regions with negative local SMB, meltwater in firn, and MOA > 0.7. This expansion will be more pronounced in Greenland than in Antarctica.

increasing shift from snowfall to rain (Fig. 6d). Surface melt is projected to extend into the interior (Fig. 6e) and the MOA = 0.7 contour moves inland, depending on future warming (Fig. 6f). The current estimates of the sea-level rise contribution of Greenland ice-sheet SMB loss in the twenty-first century are +4 ± 2 cm for Representative Concentration Pathway (RCP) 4.5 and +9 ± 4 cm for RCP 8.5 (ref. 23).

These future changes will affect firn both directly and through changes in the hydrological features of ice sheets and ice shelves[109,265]. In the lower-accumulation area of Greenland and the ice shelves of Antarctica, reduced snowfall and increased refreezing will reduce the firn thickness and air content, reducing meltwater stored by capillary forces or in aquifers[7,266]. Within Greenland, in addition to the expansion of the

## Glossary

**Ablation zone**
An ice-sheet region with negative yearly local surface mass balance.

**Accumulation**
The increase in mass at the surface of the ice sheet caused by precipitation, or the deposition of wind-transported snow.

**Atmospheric blocking**
The presence of large-scale, nearly stationary pressure anomalies generally driven by high pressure in the atmosphere, which disrupt the mean storm track and can cause persistent weather (especially temperature extremes) in a large area, lasting several days or even weeks.

**Backscatter modelling**
Modelling the interaction (reflection, refraction and scattering) of electromagnetic waves with the ice-sheet surface.

**Blue-ice areas**
Areas with sufficient negative surface mass balance to expose the bare glacial ice.

**Bucket models**
Simple description of liquid water flow in models, in which capillarity is represented by a threshold of liquid water content that must be reached in a layer before water moves downward to the layer below.

**Buried lake**
Also known as subsurface lakes. Liquid water body in the firn, formed when a surface lake freezes over and gets buried by snowfall. To be distinguished from aquifers, which denote saturation of the pore space in firn.

**Capillary barrier**
Strong contrast in capillarity between two snow layers owing to contrasting snow microstructure properties, which inhibits the downward percolation of water.

**Coffee-can method**
A method to measure firn compaction by anchoring a string or pole at the bottom of a borehole and measuring the surface-height change relative to a reference point on the string or pole. So named because the original anchors were coffee cans.

**Darcy's law**
A relationship between flow rate and pressure drop, governed by the permeability of the medium and the viscosity of the fluid that describes flow through a fully saturated porous medium.

**Deep firn cores**
Firn cores reaching deeper than approximately 15 m, such that elaborate equipment is often required to extract the core.

**Dry snow zone**
Area of the firn that remains dry throughout the year.

**Elastic properties**
Material properties that define the response of a material to the application of a force, for example by deformation or compression.

**Empirical densification laws**
Densification laws that use parameters derived from observed depth–density profiles.

**Firn air content**
A measure of the amount of air-filled pore space in the firn, computed as the volume integral over the porosity.

**Firn aquifers**
Areas inside the firn with full saturation of meltwater, which remains liquid throughout winter until the start of the next melt season.

**Fractionation**
Separation of molecules with different isotopic compositions caused by pore close-off, temperature differences or the presence of a temperature gradient.

**Glacial ice**
Part of the ice sheet where the pores in the matrix are closed off all the way to the bedrock (typical density >830 kg m$^{-3}$).

**Metamorphism**
Changes in the microstructure of firn caused by vapour transport, the presence and flow of liquid water, and variations in pressure within the snow or firn cover.

**Percolation zone**
Area of the firn with sufficient meltwater production or rainwater input to trigger downward water flow.

**Permeability**
In the context of firn, it indicates the ability of liquids and gases to move through the ice matrix.

**Permittivity**
A measure of a material's ability to interact with, and become polarized by, an applied electric field, thereby governing the transmission, reflection and absorption of electromagnetic waves in the material.

**Pore close-off**
State of the ice matrix at which the firn air becomes occluded into closed, isolated bubbles and the individual pores are no longer connected and thus cannot exchange gases, chemicals or liquid water.

**Preferential flow**
Inhomogeneous water flow in firn caused by microstructural features such as vertical pipes, small-scale spatial variability in hydraulic properties, or flow fingering resulting from instabilities in the wetting front.

**Runoff**
Liquid water leaving the firn column, firn layer or ice sheet, depending on the context. Surface runoff refers specifically to water leaving the firn at the surface.

**Runoff area**
Area of the firn in which at least some of the meltwater produced will leave the firn layer through surface runoff or drainage through the englacial drainage system in the same melt season it was produced.

**Sastrugi**
Surface snow bedform, which is widespread in environments dominated by drifting snow, characterized by elongated ridges of wind-packed snow that form owing to snow erosional processes carving into wind-packed snow.

**Semi-empirical**
Empirical approach that satisfies the principles of continuum mechanics, such as balance equations and material theory.

**Shallow firn cores**
Firn cores up to approximately 15 m depth. Typically obtained using hand drilling or only lightweight equipment.

**Sintering**
The formation and growth of bonds between snow particles.

**Slug tests**
Test to determine the horizontal hydraulic conductivity of a saturated medium by removing, adding or displacing water and monitoring the water level while equilibrium conditions return.

**Slush fields**
Areas of the firn where meltwater can be observed at the surface, suggesting a high degree of water saturation.

**Strain softening**
Reduction of a material's viscosity with increasing strain as it is deformed.

**Super-resolution downscaling**
A technique typically used in machine learning to construct high-resolution images from low-resolution images.

**Wetting front**
Separation between uniformly wet and dry firn.

ablation zone, ice slabs and other features associated with increased percolation and refreezing are expected to continue to expand to higher elevations in the interior[45].

## Summary and future perspectives

Firn is important for understanding the water budget of the Greenland and Antarctic ice sheets, correcting altimetry observations, and improving the interpretation of samples of past atmospheric composition trapped in bubbles in glacial ice. Progress in observations and model development have contributed to a relatively well-established consensus on firn compaction in the absence of liquid water. Similarly, a detailed process understanding of percolation, refreezing, and formation of meltwater features has progressively been established.

However, upscaling this knowledge from the local scale to larger (ice-sheet) scales remains a major challenge. Uncertainties stem from a limited understanding of how thick and expansive ice slabs can grow before they limit local downward percolation[267], leading to reduced water retention in the firn[258,268,269]. Current firn models struggle to reproduce ice layers in the firn and generally do not capture lateral flow[35,45,106]. Therefore, the response of the firn to predicted atmospheric warming is uncertain, especially in areas with surface melt. Nevertheless, reductions in albedo will amplify melt and decreases in FAC and permeability will reduce storage capacity[2]. These nonlinear feedbacks are expected to reduce the capacity of firn to act as a natural buffer against mass loss.

There are several avenues for further firn research that will support the monitoring and prediction of the future state of the firn layer (such as local SMB and FAC) under climate change. An advanced physical understanding of firn processes is crucial to assess the climate-change-driven transient state of the firn layer, while also making the models less reliant on tuning. The assumption of steady-state conditions, which is often made for model calibration[71,77,215], is increasingly violated owing to climate change. Additionally, the impact of extreme weather events on the firn layer could fall outside the validity range of empirical approaches. To advance physical knowledge of transient firn compaction, it is important to focus both on surface snow density as the initial condition for compaction, and on continuous field measurements of subsurface compaction. Such field measurements include strain-rate measurements using the coffee-can method[77,270–272], repeat high-resolution density measurements using neutron probes[187], phase-sensitive radio-echo sounding[273] or other indirect observations.

Laboratory experiments can also be used to understand firn processes because they enable precise control over stress and temperature, allowing expected future conditions to be sampled. Additionally, evidence of the influence of grain-scale microstructure on macroscale processes such as compaction and heat and mass flow[220,221] should encourage the use of techniques such as X-ray microtomography[191] and magnetic resonance imaging[274], to improve the physical understanding of these processes and improve firn-core analysis and model development. To improve the understanding and modelling capabilities of the fate of meltwater in connection to sea-level rise, it will be critical to develop methods to observe how deep water can percolate in wet firn in the presence of ice slabs, microstructural transitions and hydrological features such as preferential flow paths and vertical pipes[101,102,275]. The modelling of wet firn processes could build on model approaches that have been developed for seasonal snow, regarding preferential flow, lateral flow and their effects on microstructure[236,276].

The three-way integration of in situ sampling, satellite data processing and modelling should also be a key priority. For example, deriving ice-sheet mass balance and FAC from the accurate elevation change measurements from ICESat-2 requires firn models for estimating density and settling in the firn column[11,277]. Remote-sensing data can also be used to update the firn properties, such as density and optical grain size, in a model using time-dependent assimilation[278]. Such developments will require current firn model frameworks to be rethought, for example by using prognostic variables for snow microstructure that have a common basis with remote sensing, or by enabling models to be forced by observed surface-height changes.

Given the increased availability of observational data, computing resources and assimilation techniques, more thorough uncertainty bounds for model simulations should be expected. For example, Bayesian frameworks[279] could provide a probability distribution, rather than a single value, for the optimal parameter set. Such distributions can be used to calculate the uncertainties of the final firn model output. Machine learning provides another powerful avenue to exploit the wealth of remote-sensing and in situ data available, which can aid the integration of data with models through improved parameter or property estimation[280], or the analysis of large amounts of remote-sensing data. Examples of machine learning applications include, super-resolution downscaling[281] of satellite melt estimates[282], clustering techniques to identify ice-sheet surface facies[283], or classification tasks to determine the existence and spatial extent of slush fields[284] and buried lakes in firn[285]. Machine learning can also be used to create emulators, which provide a computationally efficient representation of the full (or parts, in a hybrid fashion[286]) complex physical model. Emulators can achieve simulations that are orders of magnitude faster than the original physics-based model without sacrificing much accuracy, allowing for extensive sensitivity analysis, model parameter calibration, and derivation of confidence intervals for the estimates[5,287]. All these developments benefit from sustained efforts to standardize the publication of datasets and climate model outputs, for example SUMup[288], Pangaea and the Coupled Model Intercomparison Project phase 6 (CMIP6) archive, as well as efforts to obtain different types of measurements at a single location.

To assess future sea-level change, climate models and ESMs must consider the firn layer. To calculate the mass and energy exchange at the interface between the atmosphere and the firn, the temporally varying albedo must be considered, especially in areas with melt. Additionally, the temporally and spatially varying surface roughness, which is affected by snow properties and wind processes, should be accounted for. The firn layer must be represented by multiple layers to account for prognostic density and albedo, and to consider water transport and retention[289]. The goal is for ESMs to include a dynamically evolving ice sheet to account for the melt–elevation feedback and improve predictions of sea-level change[290]. Ice-sheet models also require forcing from the heat and mass fluxes at the bottom of the firn, which impacts glacial flow. Emerging evidence that ice dynamics is affected by grain size[291] suggests that firn models that include grain size could inform the development of constitutive laws for ice deformation[291]. However, fully coupled firn model integration into ice-sheet models or the large-scale ESMs used for sea-level projections is currently rare[292].

Firn is the thin layer governing the interface between a warming climate and accelerating ice loss. Therefore, advances in understanding firn will have a crucial role in achieving accurate large-scale simulations of ice-sheet responses to global warming.

## References


1. van den Broeke, M. Depth and density of the Antarctic firn layer. *Arct. Antarct. Alp. Res.* **40**, 432–438 (2008).
2. Medley, B., Neumann, T. A., Zwally, H. J., Smith, B. E. & Stevens, C. M. Simulations of firn processes over the Greenland and Antarctic ice sheets: 1980–2021. *Cryosphere* **16**, 3971–4011 (2022).
3. Brils, M., Kuipers Munneke, P., van de Berg, W. J. & van den Broeke, M. Improved representation of the contemporary Greenland ice sheet firn layer by IMAU-FDM v1.2G. *Geosci. Model. Dev.* **15**, 7121–7138 (2022).
4. Veldhuijsen, S. B. M., van de Berg, W. J., Brils, M., Kuipers Munneke, P. & van den Broeke, M. R. Characteristics of the 1979–2020 Antarctic firn layer simulated with IMAU-FDM v1.2A. *Cryosphere* **17**, 1675–1696 (2023).
5. Verjans, V. et al. Uncertainty in East Antarctic firn thickness constrained using a model ensemble approach. *Geophys. Res. Lett.* **48**, e2020GL092060 (2021).
6. Winther, J.-G., Jespersen, M. N. & Liston, G. E. Blue-ice areas in Antarctica derived from NOAA AVHRR satellite data. *J. Glaciol.* **47**, 325–334 (2001).
7. Noël, B., Lenaerts, J. T. M., Lipscomb, W. H., Thayer-Calder, K. & van den Broeke, M. R. Peak refreezing in the Greenland firn layer under future warming scenarios. *Nat. Commun.* **13**, 6870 (2022).
8. Noël, B. et al. Modelling the climate and surface mass balance of polar ice sheets using RACMO2 — Part 1: Greenland (1958–2016). *Cryosphere* **12**, 811–831 (2018).
9. van Wessem, J. M. et al. Modelling the climate and surface mass balance of polar ice sheets using RACMO2 — Part 2: Antarctica (1979–2016). *Cryosphere* **12**, 1479–1498 (2018).
10. Shepherd, A. et al. Mass balance of the Antarctic ice sheet from 1992 to 2017. *Nature* **558**, 219–222 (2018).
11. Kuipers Munneke, P. et al. Elevation change of the Greenland Ice Sheet due to surface mass balance and firn processes, 1960–2014. *Cryosphere* **9**, 2009–2025 (2015).
12. Ligtenberg, S. R. M., Horwath, M., van den Broeke, M. R. & Legrésy, B. Quantifying the seasonal 'breathing' of the Antarctic ice sheet. *Geophys. Res. Lett.* **39**, L23501 (2012).
13. van den Broeke, M. R. et al. Contrasting current and future surface melt rates on the ice sheets of Greenland and Antarctica: lessons from in situ observations and climate models. *PLOS Clim.* **2**, e0000203 (2023).
14. Jullien, N., Tedstone, A. J., Machguth, H., Karlsson, N. B. & Helm, V. Greenland ice sheet ice slab expansion and thickening. *Geophys. Res. Lett.* **50**, e2022GL100911 (2023).
15. Miller, O. et al. Hydrology of a perennial firn aquifer in southeast Greenland: an overview driven by field data. *Water Resour. Res.* **56**, e2019WR026348 (2020).
16. Montgomery, L. N. et al. Investigation of firn aquifer structure in southeastern Greenland using active source seismology. *Front. Earth Sci*. https://doi.org/10.3389/feart.2017.00010 (2017).
17. Horlings, A. N., Christianson, K. & Miège, C. Expansion of firn aquifers in Southeast Greenland. *J. Geophys. Res. Earth Surf.* **127**, e2022JF006753 (2022).
18. Poinar, K. et al. Drainage of Southeast Greenland firn aquifer water through crevasses to the bed. *Front. Earth Sci.* **5**, 5 (2017).
19. Ligtenberg, S. R. M., van de Berg, W. J., van den Broeke, M. R., Rae, J. G. L. & van Meijgaard, E. Future surface mass balance of the Antarctic ice sheet and its influence on sea level change, simulated by a regional atmospheric climate model. *Clim. Dyn.* **41**, 867–884 (2013).
20. Lenaerts, J. T. M., Gettelman, A., Van Tricht, K., van Kampenhout, L. & Miller, N. B. Impact of cloud physics on the Greenland ice sheet near-surface climate: a study with the community atmosphere model. *J. Geophys. Res. Atmos.* **125**, e2019JD031470 (2020).
21. Vignon, É., Roussel, M.-L., Gorodetskaya, I. V., Genthon, C. & Berne, A. Present and future of rainfall in Antarctica. *Geophys. Res. Lett.* **48**, e2020GL092281 (2021).
22. Kittel, C. et al. Clouds drive differences in future surface melt over the Antarctic ice shelves. *Cryosphere* **16**, 2655–2669 (2022).
23. Fettweis, X. et al. Estimating the Greenland ice sheet surface mass balance contribution to future sea level rise using the regional atmospheric climate model MAR. *Cryosphere* **7**, 469–489 (2013).
24. Lenaerts, J. T. M., Medley, B., van den Broeke, M. R. & Wouters, B. Observing and modeling ice sheet surface mass balance. *Rev. Geophys.* **57**, 376–420 (2019).
25. Wang, W., Zender, C. S., van As, D., Fausto, R. S. & Laffin, M. K. Greenland surface melt dominated by solar and sensible heating. *Geophys. Res. Lett.* **48**, e2020GL090653 (2021).
26. Bennartz, R. et al. July 2012 Greenland melt extent enhanced by low-level liquid clouds. *Nature* **496**, 83–86 (2013).
27. Lawson, R. P. & Gettelman, A. Impact of Antarctic mixed-phase clouds on climate. *Proc. Natl. Acad. Sci. USA* **111**, 18156–18161 (2014).
28. Amory, C. et al. Seasonal variations in drag coefficient over a sastrugi-covered snowfield in coastal East Antarctica. *Bound. Layer Meteorol.* **164**, 107–133 (2017).
29. Medley, B. & Thomas, E. R. Increased snowfall over the Antarctic Ice Sheet mitigated twentieth-century sea-level rise. *Nat. Clim. Change* **9**, 34–39 (2019).
30. Nicolas, J. P. et al. January 2016 extensive summer melt in West Antarctica favoured by strong El Niño. *Nat. Commun.* **8**, 15799 (2017).
31. Goodwin, B. P., Mosley-Thompson, E., Wilson, A. B., Porter, S. E. & Sierra-Hernandez, M. R. Accumulation variability in the Antarctic Peninsula: the role of large-scale atmospheric oscillations and their interactions. *J. Clim.* **29**, 2579–2596 (2016).
32. Marshall, G. J., Thompson, D. W. J. & van den Broeke, M. R. The signature of Southern Hemisphere atmospheric circulation patterns in Antarctic precipitation. *Geophys. Res. Lett.* **44**(11), 580–11,589 (2017).
33. Pettersen, C., Henderson, S. A., Mattingly, K. S., Bennartz, R. & Breeden, M. L. The critical role of Euro-Atlantic blocking in promoting snowfall in central Greenland. *J. Geophys. Res. Atmos.* **127**, e2021JD035776 (2022).
34. Sodemann, H., Schwierz, C. & Wernli, H. Interannual variability of Greenland winter precipitation sources: Lagrangian moisture diagnostic and North Atlantic Oscillation influence. *J. Geophys. Res. Atmos*. https://doi.org/10.1029/2007JD008503 (2008).
35. Pfeffer, W. T., Meier, M. F. & Illangasekare, T. H. Retention of Greenland runoff by refreezing: implications for projected future sea level change. *J. Geophys. Res. Ocean.* **96**, 22117–22124 (1991).
36. Trusel, L. D., Frey, K. E. & Das, S. B. Antarctic surface melting dynamics: enhanced perspectives from radar scatterometer data. *J. Geophys. Res. Earth Surf*. https://doi.org/10.1029/2011JF002126 (2012).
37. Fettweis, X., Tedesco, M., van den Broeke, M. & Ettema, J. Melting trends over the Greenland ice sheet (1958–2009) from spaceborne microwave data and regional climate models. *Cryosphere* **5**, 359–375 (2011).
38. Amory, C. et al. Performance of MAR (v3.11) in simulating the drifting-snow climate and surface mass balance of Adélie Land, East Antarctica. *Geosci. Model. Dev.* **14**, 3487–3510 (2021).
39. Lenaerts, J. T. M. et al. Meltwater produced by wind–albedo interaction stored in an East Antarctic ice shelf. *Nat. Clim. Change* **7**, 58–62 (2017).
40. Arioli, S., Picard, G., Arnaud, L. & Favier, V. Dynamics of the snow grain size in a windy coastal area of Antarctica from continuous in situ spectral-albedo measurements. *Cryosphere* **17**, 2323–2342 (2023).
41. Brun, E. Investigation on wet-snow metamorphism in respect of liquid-water content. *Ann. Glaciol.* **13**, 22–26 (1989).
42. Box, J. E. et al. Greenland ice sheet albedo feedback: thermodynamics and atmospheric drivers. *Cryosphere* **6**, 821–839 (2012).
43. Jakobs, C. L., Reijmer, C. H., van den Broeke, M. R., van de Berg, W. J. & van Wessem, J. M. Spatial variability of the snowmelt–albedo feedback in Antarctica. *J. Geophys. Res. Earth Surf.* **126**, e2020JF005696 (2021).
44. Fettweis, X. et al. Reconstructions of the 1900–2015 Greenland ice sheet surface mass balance using the regional climate MAR model. *Cryosphere* **11**, 1015–1033 (2017).
45. MacFerrin, M. et al. Rapid expansion of Greenland's low-permeability ice slabs. *Nature* **573**, 403–407 (2019).
46. Machguth, H. et al. Greenland meltwater storage in firn limited by near-surface ice formation. *Nat. Clim. Change* **6**, 390–393 (2016).
47. Tedstone, A. J. & Machguth, H. Increasing surface runoff from Greenland's firn areas. *Nat. Clim. Change* **12**, 672–676 (2022).
48. Hanna, E. et al. Greenland surface air temperature changes from 1981 to 2019 and implications for ice-sheet melt and mass-balance change. *Int. J. Climatol.* **41**, E1336–E1352 (2021).
49. Tedesco, M. & Fettweis, X. Unprecedented atmospheric conditions (1948–2019) drive the 2019 exceptional melting season over the Greenland ice sheet. *Cryosphere* **14**, 1209–1223 (2020).
50. Hanna, E. et al. Atmospheric and oceanic climate forcing of the exceptional Greenland ice sheet surface melt in summer 2012. *Int. J. Climatol.* **34**, 1022–1037 (2014).
51. Wille, J. D. et al. West Antarctic surface melt triggered by atmospheric rivers. *Nat. Geosci.* **12**, 911–916 (2019).
52. Box, J. E. et al. Greenland ice sheet rainfall, heat and albedo feedback impacts from the mid-August 2021 atmospheric river. *Geophys. Res. Lett.* **49**, e2021GL097356 (2022).
53. Turner, J. et al. The dominant role of extreme precipitation events in Antarctic snowfall variability. *Geophys. Res. Lett.* **46**, 3502–3511 (2019).
54. Mattingly, K. S., Mote, T. L. & Fettweis, X. Atmospheric river impacts on Greenland ice sheet surface mass balance. *J. Geophys. Res. Atmos.* **123**, 8538–8560 (2018).
55. Wille, J. D. et al. Antarctic atmospheric river climatology and precipitation impacts. *J. Geophys. Res. Atmos.* **126**, e2020JD033788 (2021).
56. Maclennan, M. L. et al. Climatology and surface impacts of atmospheric rivers on West Antarctica. *Cryosphere* **17**, 865–881 (2023).
57. Hofer, S., Tedstone, A. J., Fettweis, X. & Bamber, J. L. Decreasing cloud cover drives the recent mass loss on the Greenland ice sheet. *Sci. Adv.* **3**, e1700584 (2017).
58. Xu, Z., Han, Y., Tam, C.-Y., Yang, Z.-L. & Fu, C. Bias-corrected CMIP6 global dataset for dynamical downscaling of the historical and future climate (1979–2100). *Sci. Data* **8**, 293 (2021).
59. Krinner, G. & Flanner, M. G. Striking stationarity of large-scale climate model bias patterns under strong climate change. *Proc. Natl. Acad. Sci. USA* **115**, 9462–9466 (2018).
60. Hofer, S., Tedstone, A. J., Fettweis, X. & Bamber, J. L. Cloud microphysics and circulation anomalies control differences in future Greenland melt. *Nat. Clim. Change* **9**, 523–528 (2019).
61. Delhasse, A., Hanna, E., Kittel, C. & Fettweis, X. Brief communication: CMIP6 does not suggest any atmospheric blocking increase in summer over Greenland by 2100. *Int. J. Climatol.* **41**, 2589–2596 (2021).
62. Colbeck, S. C. Sintering in a dry snow cover. *J. Appl. Phys.* **84**, 4585–4589 (1998).
63. Alley, R. B. Firn densification by grain-boundary sliding: a first model. *J. Phys. Colloq.* **48**, C1–256 (1987).
64. Calonne, N. et al. 3-D image-based numerical computations of snow permeability: links to specific surface area, density, and microstructural anisotropy. *Cryosphere* **6**, 939–951 (2012).
65. Spaulding, N. E., Meese, D. A. & Baker, I. Advanced microstructural characterization of four East Antarctic firn/ice cores. *J. Glaciol.* **57**, 796–810 (2011).

66. Vionnet, V. et al. The detailed snowpack scheme Crocus and its implementation in SURFEX v7.2. *Geosci. Model. Dev.* **5**, 773–791 (2012).
67. Helfricht, K., Hartl, L., Koch, R., Marty, C. & Olefs, M. Obtaining sub-daily new snow density from automated measurements in high mountain regions. *Hydrol. Earth Syst. Sci.* **22**, 2655–2668 (2018).
68. Wever, N. et al. Observations and simulations of new snow density in the drifting snow-dominated environment of Antarctica. *J. Glaciol.* **69**, 823–840 (2022).
69. Colbeck, S. C. An overview of seasonal snow metamorphism. *Rev. Geophys.* **20**, 45–61 (1982).
70. van Kampenhout, L. et al. Improving the representation of polar snow and firn in the Community Earth System Model. *J. Adv. Model. Earth Syst.* **9**, 2583–2600 (2017).
71. Herron, M. M. & Langway, C. C. Firn densification: an empirical model. *J. Glaciol.* **25**, 373–385 (1980).
72. Maeno, N. & Ebinuma, T. Pressure sintering of ice and its implication to the densification of snow at polar glaciers and ice sheets. *J. Phys. Chem.* **87**, 4103–4110 (1983).
73. Benson, C. S. *Stratigraphic Studies in the Snow and Firn of the Greenland Ice Sheet.*PhD thesis, California Institute of Technology https://doi.org/10.7907/G7V2-0T57 (1960).
74. Colbeck, S. C. & Parssinen, N. Regelation and the deformation of wet snow. *J. Glaciol.* **21**, 639–650 (1978).
75. Flanner, M. G. & Zender, C. S. Linking snowpack microphysics and albedo evolution. *J. Geophys. Res. Atmos.* https://doi.org/10.1029/2005JD006834 (2006).
76. Calonne, N. et al. Thermal conductivity of snow, firn, and porous ice from 3-D image-based computations. *Geophys. Res. Lett.* **46**, 13079–13089 (2019).
77. Arthern, R. J., Vaughan, D. G., Rankin, A. M., Mulvaney, R. & Thomas, E. R. In situ measurements of Antarctic snow compaction compared with predictions of models. *J. Geophys. Res. Earth Surf.* https://doi.org/10.1029/2009JF001306 (2010).
78. Meyer, C. R., Keegan, K. M., Baker, I. & Hawley, R. L. A model for French-press experiments of dry snow compaction. *Cryosphere* **14**, 1449–1458 (2020).
79. Morris, E. M. & Wingham, D. J. Densification of polar snow: measurements, modeling, and implications for altimetry. *J. Geophys. Res. Earth Surf.* **119**, 349–365 (2014).
80. Lehning, M., Bartelt, P., Brown, B., Fierz, C. & Satyawali, P. A physical SNOWPACK model for the Swiss avalanche warning: Part II. Snow microstructure. *Cold Reg. Sci. Technol.* **35**, 147–167 (2002).
81. Blackford, J. R. Sintering and microstructure of ice: a review. *J. Phys. Appl. Phys.* **40**, R355 (2007).
82. Gow, A. J. On the rates of growth of grains and crystals in south polar firn. *J. Glaciol.* **8**, 241–252 (1969).
83. Stephenson, A. J. Some consideration of snow metamorphism in the Antarctic ice sheet in the light of ice crystal studies. *Phys. Snow Ice* **1**, 725–740 (1967).
84. Adolph, A. & Albert, M. R. An improved technique to measure firn diffusivity. *Int. J. Heat. Mass. Transf.* **61**, 598–604 (2013).
85. Gregory, S. A., Albert, M. R. & Baker, I. Impact of physical properties and accumulation rate on pore close-off in layered firn. *Cryosphere* **8**, 91–105 (2014).
86. Courville, Z., Hörhold, M., Hopkins, M. & Albert, M. Lattice-Boltzmann modeling of the air permeability of polar firn. *J. Geophys. Res. Earth Surf.* https://doi.org/10.1029/2009JF001549 (2010).
87. Albert, M. R. & Shultz, E. F. Snow and firn properties and air–snow transport processes at Summit, Greenland. *Atmos. Environ.* **36**, 2789–2797 (2002).
88. Albert, M. R. & Hawley, R. L. Seasonal changes in snow surface roughness characteristics at Summit, Greenland: implications for snow and firn ventilation. *Ann. Glaciol.* **35**, 510–514 (2002).
89. Fettweis, X. et al. GrSMBMIP: intercomparison of the modelled 1980–2012 surface mass balance over the Greenland Ice Sheet. *Cryosphere* **14**, 3935–3958 (2020).
90. Mouginot, J. et al. Forty-six years of Greenland ice sheet mass balance from 1972 to 2018. *Proc. Natl. Acad. Sci. USA* **116**, 9239–9244 (2019).
91. Agosta, C. et al. Estimation of the Antarctic surface mass balance using the regional climate model MAR (1979–2015) and identification of dominant processes. *Cryosphere* **13**, 281–296 (2019).
92. Yamaguchi, S., Watanabe, K., Katsushima, T., Sato, A. & Kumakura, T. Dependence of the water retention curve of snow on snow characteristics. *Ann. Glaciol.* **53**, 6–12 (2012).
93. Colbeck, S. C. The capillary effects on water percolation in homogeneous snow. *J. Glaciol.* **13**, 85–97 (1974).
94. Illangasekare, T. H., Walter, R. J. Jr., Meier, M. F. & Pfeffer, W. T. Modeling of meltwater infiltration in subfreezing snow. *Water Resour. Res.* **26**, 1001–1012 (1990).
95. Meyer, C. R. & Hewitt, I. J. A continuum model for meltwater flow through compacting snow. *Cryosphere* **11**, 2799–2813 (2017).
96. Avanzi, F., Hirashima, H., Yamaguchi, S., Katsushima, T. & De Michele, C. Observations of capillary barriers and preferential flow in layered snow during cold laboratory experiments. *Cryosphere* **10**, 2013–2026 (2016).
97. Cueto-Felgueroso, L. & Juanes, R. A phase field model of unsaturated flow. *Water Resour. Res.* https://doi.org/10.1029/2009WR007945 (2009).
98. Jordan, R. Effects of capillary discontinuities on water flow retention in layered snow covers. *Def. Sci. J.* **45**, 79–91 (1995).
99. Hirashima, H., Avanzi, F. & Wever, N. Wet-snow metamorphism drives the transition from preferential to matrix flow in snow. *Geophys. Res. Lett.* **46**, 14548–14557 (2019).
100. Humphrey, N. F., Harper, J. T. & Pfeffer, W. T. Thermal tracking of meltwater retention in Greenland's accumulation area. *J. Geophys. Res. Earth Surf.* https://doi.org/10.1029/2011JF002083 (2012).
101. Heilig, A., Eisen, O., MacFerrin, M., Tedesco, M. & Fettweis, X. Seasonal monitoring of melt and accumulation within the deep percolation zone of the Greenland ice sheet and comparison with simulations of regional climate modeling. *Cryosphere* **12**, 1851–1866 (2018).
102. Humphrey, N. F., Harper, J. T. & Meierbachtol, T. W. Physical limits to meltwater penetration in firn. *J. Glaciol.* **67**, 952–960 (2021).
103. Pfeffer, W. T. & Humphrey, N. F. Determination of timing and location of water movement and ice-layer formation by temperature measurements in sub-freezing snow. *J. Glaciol.* **42**, 292–304 (1996).
104. Vandecrux, B. et al. Firn cold content evolution at nine sites on the Greenland ice sheet between 1998 and 2017. *J. Glaciol.* **66**, 591–602 (2020).
105. Braithwaite, R. J., Laternser, M. & Pfeffer, W. T. Variations of near-surface firn density in the lower accumulation area of the Greenland ice sheet, Pâkitsoq, West Greenland. *J. Glaciol.* **40**, 477–485 (1994).
106. Harper, J., Humphrey, N., Pfeffer, W. T., Brown, J. & Fettweis, X. Greenland ice-sheet contribution to sea-level rise buffered by meltwater storage in firn. *Nature* **491**, 240–243 (2012).
107. Miège, C. et al. Spatial extent and temporal variability of Greenland firn aquifers detected by ground and airborne radars. *J. Geophys. Res. Earth Surf.* **121**, 2381–2398 (2016).
108. Forster, R. R. et al. Extensive liquid meltwater storage in firn within the Greenland ice sheet. *Nat. Geosci.* **7**, 95–98 (2014).
109. Bell, R. E., Banwell, A. F., Trusel, L. D. & Kingslake, J. Antarctic surface hydrology and impacts on ice-sheet mass balance. *Nat. Clim. Change* **8**, 1044–1052 (2018).
110. Warner, R. C. et al. rapid formation of an ice doline on Amery Ice Shelf, East Antarctica. *Geophys. Res. Lett.* **48**, e2020GL091095 (2021).
111. Culberg, R., Chu, W. & Schroeder, D. M. Shallow fracture buffers high elevation runoff in northwest Greenland. *Geophys. Res. Lett.* **49**, e2022GL101151 (2022).
112. Das, S. B. et al. Fracture propagation to the base of the Greenland ice sheet during supraglacial lake drainage. *Science* **320**, 778–781 (2008).
113. Koenig, L. S. et al. Wintertime storage of water in buried supraglacial lakes across the Greenland ice sheet. *Cryosphere* **9**, 1333–1342 (2015).
114. Hubbard, B. et al. Massive subsurface ice formed by refreezing of ice-shelf melt ponds. *Nat. Commun.* **7**, 11897 (2016).
115. Munneke, P. K. M., Ligtenberg, S. R., van den Broeke, M. R., van Angelen, J. H. & Forster, R. R. Explaining the presence of perennial liquid water bodies in the firn of the Greenland ice sheet. *Geophys. Res. Lett.* **41**, 476–483 (2014).
116. Koenig, L. S., Miège, C., Forster, R. R. & Brucker, L. Initial in situ measurements of perennial meltwater storage in the Greenland firn aquifer. *Geophys. Res. Lett.* **41**, 81–85 (2014).
117. Miller, O. et al. Direct evidence of meltwater flow within a firn aquifer in southeast Greenland. *Geophys. Res. Lett.* **45**, 207–215 (2018).
118. Chu, W., Schroeder, D. M., & Siegfried, M. R. Retrieval of englacial firn aquifer thickness from ice-penetrating radar sounding in southeastern Greenland. *Geophys. Res. Lett.* **45**, 11770–11778 (2018).
119. Poinar, K., Dow, C. F. & Andrews, L. C. Long-term support of an active subglacial hydrologic system in southeast Greenland by firn aquifers. *Geophys. Res. Lett.* **46**, 4772–4781 (2019).
120. Montgomery, L. et al. Hydrologic properties of a highly permeable firn aquifer in the Wilkins ice shelf, Antarctica. *Geophys. Res. Lett.* **47**, e2020GL089552 (2020).
121. Fausto, R. S. et al. Programme for Monitoring of the Greenland Ice Sheet (PROMICE) automatic weather station data. *Earth Syst. Sci. Data* **13**, 3819–3845 (2021).
122. Smeets, P. C. J. P. et al. The K-transect in west Greenland: automatic weather station data (1993–2016). *Arct. Antarct. Alp. Res.* **50**, S100002 (2018).
123. Wang, Y. et al. The AntAWS dataset: a compilation of Antarctic automatic weather station observations. *Earth Syst. Sci. Data* **15**, 411–429 (2023).
124. Järvinen, O., Leppäranta, M. & Vehviläinen, J. One-year records from automatic snow stations in western Dronning Maud Land, Antarctica. *Antarct. Sci.* **25**, 711–728 (2013).
125. Kuipers Munneke, P. et al. Observationally constrained surface mass balance of Larsen C ice shelf, Antarctica. *Cryosphere* **11**, 2411–2426 (2017).
126. Rennermalm, Å. K. et al. Shallow firn cores 1989–2019 in southwest Greenland's percolation zone reveal decreasing density and ice layer thickness after 2012. *J. Glaciol.* **68**, 431–442 (2022).
127. Vandecrux, B. et al. Firn data compilation reveals widespread decrease of firn air content in western Greenland. *Cryosphere* **13**, 845–859 (2019).
128. Thomas, E. R. et al. Regional Antarctic snow accumulation over the past 1000 years. *Clim. Past.* **13**, 1491–1513 (2017).
129. Brown, J., Harper, J., Pfeffer, W. T., Humphrey, N. & Bradford, J. High-resolution study of layering within the percolation and soaked facies of the Greenland ice sheet. *Ann. Glaciol.* **52**, 35–42 (2011).
130. Eisen, O., Wilhelms, F., Nixdorf, U. & Miller, H. Identifying isochrones in GPR profiles from DEP-based forward modeling. *Ann. Glaciol.* **37**, 344–350 (2003).
131. Arcone, S. A., Spikes, V. B. & Hamilton, G. S. Stratigraphic variation within polar firn caused by differential accumulation and ice flow: interpretation of a 400 MHz short-pulse radar profile from West Antarctica. *J. Glaciol.* **51**, 407–422 (2005).
132. Meehan, T. G. et al. Reconstruction of historical surface mass balance, 1984–2017 from GreenTrACS multi-offset ground-penetrating radar. *J. Glaciol.* **67**, 219–228 (2021).
133. Kruetzmann, N. C., Rack, W., McDonald, A. J. & George, S. E. Snow accumulation and compaction derived from GPR data near Ross Island, Antarctica. *Cryosphere* **5**, 391–404 (2011).

134. Case, E. & Kingslake, J. Phase-sensitive radar as a tool for measuring firn compaction. *J. Glaciol.* **68**, 139–152 (2022).
135. Drews, R. et al. Constraining variable density of ice shelves using wide-angle radar measurements. *Cryosphere* **10**, 811–823 (2016).
136. Robin, G. de Q. Seismic shooting and related investigations. In *Norwegian–British–Swedish Antarctic Expedition, 1949–52: Scientific Results* Vol. 5 (Norsk Polarinstituttt, 1958).
137. Kovacs, A., Gow, A. J. & Morey, R. M. The in-situ dielectric constant of polar firn revisited. *Cold Reg. Sci. Technol.* **23**, 245–256 (1995).
138. Diez, A. et al. Ice shelf structure derived from dispersion curve analysis of ambient seismic noise, Ross Ice Shelf, Antarctica. *Geophys. J. Int.* **205**, 785–795 (2016).
139. Chaput, J., Aster, R., Karplus, M. & Nakata, N. Ambient high-frequency seismic surface waves in the firn column of central west Antarctica. *J. Glaciol.* **68**, 785–798 (2022).
140. Zhou, W. et al. Seismic noise interferometry and distributed acoustic sensing (DAS): inverting for the firn layer S-velocity structure on Rutford ice stream, Antarctica. *J. Geophys. Res. Earth Surf.* **127**, e2022JF006917 (2022).
141. Diez, A. et al. Influence of ice crystal anisotropy on seismic velocity analysis. *Ann. Glaciol.* **55**, 97–106 (2014).
142. Pearce, E. et al. Characterising ice slabs in firn using seismic full waveform inversion, a sensitivity study. *J. Glaciol.* **69**, 1419–1433 (2023).
143. Schlegel, R. et al. Comparison of elastic moduli from seismic diving-wave and ice-core microstructure analysis in Antarctic polar firn. *Ann. Glaciol.* **60**, 220–230 (2019).
144. King, E. C. & Jarvis, E. P. Use of shear waves to measure Poisson's ratio in polar firn. *J. Environ. Eng. Geophys.* **12**, 15–21 (2007).
145. Smith, E. C. et al. Ice fabric in an Antarctic ice stream interpreted from seismic anisotropy. *Geophys. Res. Lett.* **44**, 3710–3718 (2017).
146. Llorens, M.-G. et al. Can changes in deformation regimes be inferred from crystallographic preferred orientations in polar ice? *Cryosphere* **16**, 2009–2024 (2022).
147. Hollmann, H., Treverrow, A., Peters, L. E., Reading, A. M. & Kulessa, B. Seismic observations of a complex firn structure across the Amery ice shelf, East Antarctica. *J. Glaciol.* **67**, 777–787 (2021).
148. Otosaka, I. N. et al. Surface melting drives fluctuations in airborne radar penetration in west central Greenland. *Geophys. Res. Lett.* **47**, e2020GL088293 (2020).
149. Pritchard, H. D., Arthern, R. J., Vaughan, D. G. & Edwards, L. A. Extensive dynamic thinning on the margins of the Greenland and Antarctic ice sheets. *Nature* **461**, 971–975 (2009).
150. Smith, B. et al. Pervasive ice sheet mass loss reflects competing ocean and atmosphere processes. *Science* **368**, 1239–1242 (2020).
151. Helm, V., Humbert, A. & Miller, H. Elevation and elevation change of Greenland and Antarctica derived from CryoSat-2. *Cryosphere* **8**, 1539–1559 (2014).
152. McMillan, M. et al. A high-resolution record of Greenland mass balance. *Geophys. Res. Lett.* **43**, 7002–7010 (2016).
153. Simonsen, S. B. & Sørensen, L. S. Implications of changing scattering properties on Greenland ice sheet volume change from CryoSat-2 altimetry. *Remote. Sens. Environ.* **190**, 207–216 (2017).
154. Reeh, N. A nonsteady-state firn-densification model for the percolation zone of a glacier. *J. Geophys. Res. Earth Surf.* https://doi.org/10.1029/2007JF00074 (2008).
155. Helsen, M. M. et al. Elevation changes in Antarctica mainly determined by accumulation variability. *Science* **320**, 1626–1629 (2008).
156. Sørensen, L. S. et al. Mass balance of the Greenland ice sheet (2003–2008) from ICESat data — the impact of interpolation, sampling and firn density. *Cryosphere* **5**, 173–186 (2011).
157. Zwally, H. J. et al. Greenland ice sheet mass balance: distribution of increased mass loss with climate warming; 2003–07 versus 1992–2002. *J. Glaciol.* **57**, 88–102 (2011).
158. Grima, C., Blankenship, D. D., Young, D. A. & Schroeder, D. M. Surface slope control on firn density at Thwaites Glacier, West Antarctica: results from airborne radar sounding. *Geophys. Res. Lett.* **41**, 6787–6794 (2014).
159. Simonsen, S. B. et al. Assessing a multilayered dynamic firn-compaction model for Greenland with ASIRAS radar measurements. *J. Glaciol.* **59**, 545–558 (2013).
160. Medley, B. et al. Antarctic firn compaction rates from repeat-track airborne radar data: I. Methods. *Ann. Glaciol.* **56**, 155–166 (2015).
161. Scanlan, K. M., Rutishauser, A. & Simonsen, S. B. Observing the near-surface properties of the Greenland ice sheet. *Geophys. Res. Lett.* **50**, e2022GL101702 (2023).
162. Kuipers Munneke, P. et al. The K-transect on the western Greenland ice sheet: surface energy balance (2003–2016). *Arct. Antarct. Alp. Res.* **50**, e1420952 (2018).
163. Sihvola, A. & Tiuri, M. Snow fork for field determination of the density and wetness profiles of a snow pack. *IEEE Trans. Geosci. Remote. Sens.* **GE-24**, 717–721 (1986).
164. Tiuri, M., Sihvola, A., Nyfors, E. & Hallikaiken, M. The complex dielectric constant of snow at microwave frequencies. *IEEE J. Ocean. Eng.* **9**, 377–382 (1984).
165. Kendra, J. R., Ulaby, F. T. & Sarabandi, K. Snow probe for in situ determination of wetness and density. *IEEE Trans. Geosci. Remote. Sens.* **32**, 1152–1159 (1994).
166. Techel, F. & Pielmeier, C. Point observations of liquid water content in wet snow — investigating methodical, spatial and temporal aspects. *Cryosphere* **5**, 405–418 (2011).
167. Fahnestock, M., Bindschadler, R., Kwok, R. & Jezek, K. Greenland ice sheet surface properties and ice dynamics from ERS-1 SAR imagery. *Science* **262**, 1530–1534 (1993).
168. Alley, K. E., Scambos, T. A., Miller, J. Z., Long, D. G. & MacFerrin, M. Quantifying vulnerability of Antarctic ice shelves to hydrofracture using microwave scattering properties. *Remote Sens. Environ.* **210**, 297–306 (2018).
169. Bell, C. et al. Spatial and temporal variability in the snowpack of a High Arctic ice cap: implications for mass-change measurements. *Ann. Glaciol.* **48**, 159–170 (2008).
170. Campbell, J. L., Mitchell, M. J., Mayer, B., Groffman, P. M. & Christenson, L. M. Mobility of nitrogen-15-labeled nitrate and sulfur-34-labeled sulfate during snowmelt. *Soil. Sci. Soc. Am. J.* **71**, 1934–1944 (2007).
171. Clerx, N. et al. In situ measurements of meltwater flow through snow and firn in the accumulation zone of the SW Greenland ice sheet. *Cryosphere* **16**, 4379–4401 (2022).
172. Miller, O. L. et al. Hydraulic conductivity of a firn aquifer in southeast Greenland. *Front. Earth Sci.* **5**, 38 (2017).
173. Kulessa, B., Chandler, D., Revil, A. & Essery, R. Theory and numerical modeling of electrical self-potential signatures of unsaturated flow in melting snow. *Water Resour. Res.* **48**, https://doi.org/10.1029/2012WR012048 (2012).
174. Thompson, S. S., Kulessa, B., Essery, R. L. H. & Lüthi, M. P. Bulk meltwater flow and liquid water content of snowpacks mapped using the electrical self-potential (SP) method. *Cryosphere* **10**, 433–444 (2016).
175. Sommers, A. N. et al. Inferring firn permeability from pneumatic testing: a case study on the Greenland ice sheet. *Front. Earth Sci.* **5**, 20 (2017).
176. St. Clair, J. & Holbrook, W. S. Measuring snow water equivalent from common-offset GPR records through migration velocity analysis. *Cryosphere* **11**, 2997–3009 (2017).
177. Bradford, J. H., Harper, J. T. & Brown, J. Complex dielectric permittivity measurements from ground-penetrating radar data to estimate snow liquid water content in the pendular regime. *Water Resour. Res.* https://doi.org/10.1029/2009WR008959 (2009).
178. Killingbeck, S. F. et al. Integrated borehole, radar, and seismic velocity analysis reveals dynamic spatial variations within a firn aquifer in southeast Greenland. *Geophys. Res. Lett.* **47**, e2020GL089335 (2020).
179. Legchenko, A. et al. Estimating water volume stored in the south-eastern Greenland firn aquifer using magnetic-resonance soundings. *J. Appl. Geophys.* **150**, 11–20 (2018).
180. Brangers, I. et al. Sentinel-1 detects firn aquifers in the Greenland ice sheet. *Geophys. Res. Lett.* **47**, e2019GL085192 (2020).
181. Kar, R., Aksoy, M., Kaurejo, D., Atrey, P. & Devadason, J. A. Antarctic firn characterization via wideband microwave radiometry. *Remote Sens.* **14**, 2258 (2022).
182. Naderpour, R. & Schwank, M. Snow wetness retrieved from L-band radiometry. *Remote. Sens.* **10**, 359 (2018).
183. Tape, K. D., Rutter, N., Marshall, H.-P., Essery, R. & Sturm, M. Recording microscale variations in snowpack layering using near-infrared photography. *J. Glaciol.* **56**, 75–80 (2010).
184. Dey, R. et al. Application of visual stratigraphy from line-scan images to constrain chronology and melt features of a firn core from coastal Antarctica. *J. Glaciol.* **69**, 179–190 (2023).
185. Sigl, M. et al. The WAIS divide deep ice core WD2014 chronology — Part 2: annual-layer counting (0–31 ka BP). *Clim. Past.* **12**, 769–786 (2016).
186. Nye, J. F. Correction factor for accumulation measured by the thickness of the annual layers in an ice sheet. *J. Glaciol.* **4**, 785–788 (1963).
187. Morris, E. M. & Cooper, J. D. Density measurements in ice boreholes using neutron scattering. *J. Glaciol.* **49**, 599–604 (2003).
188. Hori, A. et al. A detailed density profile of the Dome Fuji (Antarctica) shallow ice core by X-ray transmission method. *Ann. Glaciol.* **29**, 211–214 (1999).
189. Gerland, S. et al. Density log of a 181 m long ice core from Berkner Island, Antarctica. *Ann. Glaciol.* **29**, 215–219 (1999).
190. Sjögren, B. et al. Determination of firn density in ice cores using image analysis. *J. Glaciol.* **53**, 413–419 (2007).
191. Burr, A., Lhuissier, P., Martin, C. L. & Philip, A. In situ X-ray tomography densification of firn: the role of mechanics and diffusion processes. *Acta Mater.* **167**, 210–220 (2019).
192. Alley, R. B. & Anandakrishnan, S. Variations in melt-layer frequency in the GISP2 ice core: implications for Holocene summer temperatures in central Greenland. *Ann. Glaciol.* **21**, 64–70 (1995).
193. Parry, V. et al. Investigations of meltwater refreezing and density variations in the snowpack and firn within the percolation zone of the Greenland ice sheet. *Ann. Glaciol.* **46**, 61–68 (2007).
194. MacDonell, S., Fernandoy, F., Villar, P. & Hammann, A. Stratigraphic analysis of firn cores from an Antarctic ice shelf firn aquifer. *Water* **13**, 731 (2021).
195. Schwander, J. & Stauffer, B. Age difference between polar ice and the air trapped in its bubbles. *Nature* **311**, 45–47 (1984).
196. Sowers, T., Bender, M., Raynaud, D. & Korotkevich, Y. S. $\delta^{15}N$ of $N_2$ in air trapped in polar ice: a tracer of gas transport in the firn and a possible constraint on ice age–gas age differences. *J. Geophys. Res. Atmos.* **97**, 15683–15697 (1992).
197. Severinghaus, J. P., Sowers, T., Brook, E. J., Alley, R. B. & Bender, M. L. Timing of abrupt climate change at the end of the Younger Dryas interval from thermally fractionated gases in polar ice. *Nature* **391**, 141–146 (1998).
198. Suwa, M. & Bender, M. L. $O_2/N_2$ ratios of occluded air in the GISP2 ice core. *J. Geophys. Res. Atmos.* https://doi.org/10.1029/2007JD009589 (2008).
199. Huber, C. et al. Isotope calibrated Greenland temperature record over Marine Isotope Stage 3 and its relation to $CH_4$. *Earth Planet. Sci. Lett.* **243**, 504–519 (2006).
200. Kawamura, K. et al. Northern hemisphere forcing of climatic cycles in Antarctica over the past 360,000 years. *Nature* **448**, 912–916 (2007).
201. Bender, M. L. Orbital tuning chronology for the Vostok climate record supported by trapped gas composition. *Earth Planet. Sci. Lett.* **204**, 275–289 (2002).
202. Fujita, S., Okuyama, J., Hori, A. & Hondoh, T. Metamorphism of stratified firn at Dome Fuji, Antarctica: a mechanism for local insolation modulation of gas transport conditions during bubble close off. *J. Geophys. Res. Earth Surf.* https://doi.org/10.1029/2008JF001143 (2009).

203. Baggenstos, D. et al. A horizontal ice core from Taylor Glacier, its implications for Antarctic climate history, and an improved Taylor Dome ice core time scale. *Paleoceanogr. Paleoclimatol.* **33**, 778–794 (2018).
204. Buizert, C. The ice core gas age–ice age difference as a proxy for surface temperature. *Geophys. Res. Lett.* **48**, e2021GL094241 (2021).
205. Buizert, C. et al. Antarctic surface temperature and elevation during the Last Glacial Maximum. *Science* **372**, 1097–1101 (2021).
206. Cuffey, K. M. et al. Large Arctic temperature change at the Wisconsin-Holocene glacial transition. *Science* **270**, 455–458 (1995).
207. Cuffey, K. M. et al. Deglacial temperature history of West Antarctica. *Proc. Natl Acad. Sci.* **113**, 14249–14254 (2016).
208. Schwander, J. et al. Age scale of the air in the summit ice: implication for glacial–interglacial temperature change. *J. Geophys. Res. Atmos.* **102**, 19483–19493 (1997).
209. Landais, A. et al. Firn-air $\delta^{15}$N in modern polar sites and glacial–interglacial ice: a model-data mismatch during glacial periods in Antarctica? *Quat. Sci. Rev.* **25**, 49–62 (2006).
210. Lundin, J. M. D. et al. Firn Model Intercomparison Experiment (FirnMICE). *J. Glaciol.* **63**, 401–422 (2017).
211. Morland, L. W., Kelly, R. J. & Morris, E. M. A mixture theory for a phase-changing snowpack. *Cold Reg. Sci. Technol.* **17**, 271–285 (1990).
212. Stevens, C. M. et al. The Community Firn Model (CFM) v1.0. *Geosci. Model. Dev.* **13**, 4355–4377 (2020).
213. Bader, H. Sorge's law of densification of snow on high polar glaciers. *J. Glaciol.* **2**, 319–323 (1954).
214. Kingslake, J., Skarbek, R., Case, E. & McCarthy, C. Grain-size evolution controls the accumulation dependence of modelled firn thickness. *Cryosphere* **16**, 3413–3430 (2022).
215. Ligtenberg, S. R. M., Helsen, M. M. & van den Broeke, M. R. An improved semi-empirical model for the densification of Antarctic firn. *Cryosphere* **5**, 809–819 (2011).
216. Barnola, J.-M., Pimienta, P., Raynaud, D. & Korotkevich, Y. S. $CO_2$–climate relationship as deduced from the Vostok ice core: a re-examination based on new measurements and on a re-evaluation of the air dating. *Tellus B* **43**, 83 (1991).
217. Goujon, C., Barnola, J.-M. & Ritz, C. Modeling the densification of polar firn including heat diffusion: application to close-off characteristics and gas isotopic fractionation for Antarctica and Greenland sites. *J. Geophys. Res. Atmos.* **108**, 4792 (2003).
218. Wilkinson, D. S. A pressure-sintering model for the densification of polar firn and glacier ice. *J. Glaciol.* **34**, 40–45 (1988).
219. Arnaud, L., Barnola, J.-M. & Duval, P. in *Physics of Ice Core Records*, 285–305 (Hokkaido Univ. Press, 2000).
220. Theile, T., Löwe, H., Theile, T. C. & Schneebeli, M. Simulating creep of snow based on microstructure and the anisotropic deformation of ice. *Acta Mater.* **59**, 7104–7113 (2011).
221. Fourteau, K., Gillet-Chaulet, F., Martinerie, P. & Faïn, X. A micro-mechanical model for the transformation of dry polar firn into ice using the level-set method. *Front. Earth Sci.* **8**, 101 (2020).
222. Salamating, A. N. et al. in *Physics of Ice Records II*, Vol. 68, 195–222 (Hokkaido Univ. Press, 2009).
223. Hörhold, M. W., Kipfstuhl, S., Wilhelms, F., Freitag, J. & Frenzel, A. The densification of layered polar firn. *J. Geophys. Res. Earth Surf*. https://doi.org/10.1029/2009JF001630 (2011).
224. Schultz, T., Müller, R., Gross, D. & Humbert, A. On the contribution of grain boundary sliding type creep to firn densification — an assessment using an optimization approach. *Cryosphere* **16**, 143–158 (2022).
225. Morris, E. M., Montgomery, L. N. & Mulvaney, R. Modelling the transition from grain-boundary sliding to power-law creep in dry snow densification. *J. Glaciol.* **68**, 417–430 (2022).
226. Arnaud, L., Lipenkov, V., Barnola, J. M., Gay, M. & Duval, P. Modelling of the densification of polar firn: characterization of the snow–firn transition. *Ann. Glaciol.* **26**, 39–44 (1998).
227. Bréant, C., Martinerie, P., Orsi, A., Arnaud, L. & Landais, A. Modelling firn thickness evolution during the last deglaciation: constraints on sensitivity to temperature and impurities. *Clim. Past.* **13**, 833–853 (2017).
228. Freitag, J., Kipfstuhl, S., Laepple, T. & Wilhelms, F. Impurity-controlled densification: a new model for stratified polar firn. *J. Glaciol.* **59**, 1163–1169 (2013).
229. Morris, E. M. et al. Snow densification and recent accumulation along the iSTAR Traverse, Pine Island Glacier, Antarctica. *J. Geophys. Res. Earth Surf.* **122**, 2284–2301 (2017).
230. Horlings, A. N., Christianson, K., Holschuh, N., Stevens, C. M. & Waddington, E. D. Effect of horizontal divergence on estimates of firn-air content. *J. Glaciol.* **67**, 287–296 (2021).
231. Oraschewski, F. M. & Grinsted, A. Modeling enhanced firn densification due to strain softening. *Cryosphere* **16**, 2683–2700 (2022).
232. Gagliardini, O. & Meyssonnier, J. Flow simulation of a firn-covered cold glacier. *Ann. Glaciol.* **24**, 242–248 (1997).
233. Vandecrux, B. et al. The firn meltwater Retention Model Intercomparison Project (RetMIP): evaluation of nine firn models at four weather station sites on the Greenland ice sheet. *Cryosphere* **14**, 3785–3810 (2020).
234. Wever, N., Fierz, C., Mitterer, C., Hirashima, H. & Lehning, M. Solving Richards equation for snow improves snowpack meltwater runoff estimations in detailed multi-layer snowpack model. *Cryosphere* **8**, 257–274 (2014).
235. Gray, J. M. N. T. Water movement in wet snow. *Philos. Trans. R. Soc. Lond. A* **354**, 465–500 (1997).
236. Wever, N., Würzer, S., Fierz, C. & Lehning, M. Simulating ice layer formation under the presence of preferential flow in layered snowpacks. *Cryosphere* **10**, 2731–2744 (2016).
237. Schneebeli, M. Development and stability of preferential flow paths in a layered snowpack. *Biochem. Seas. Snow Cover. Catchments* **228**, 89–95 (1995).
238. Marchenko, S. et al. Parameterizing deep water percolation improves subsurface temperature simulations by a multilayer firn model. *Front. Earth Sci*. https://doi.org/10.3389/feart.2017.00016 (2017).
239. Leroux, N. R., Marsh, C. B. & Pomeroy, J. W. Simulation of preferential flow in snow with a 2-D non-equilibrium Richards model and evaluation against laboratory data. *Water Resour. Res.* **56**, e2020WR027466 (2020).
240. Steger, C. R. et al. Firn meltwater retention on the Greenland ice sheet: a model comparison. *Front. Earth Sci.* **5**, 3 (2017).
241. Miller, O. et al. Hydrologic modeling of a perennial firn aquifer in southeast Greenland. *J. Glaciol.* **69**, 607–622 (2023).
242. Buizert, C. Ice core methods — studies of firn air. In *Encyclopedia of Quaternary Science*, 361–372 (Elsevier, 2013).
243. Rommelaere, V., Arnaud, L. & Barnola, J.-M. Reconstructing recent atmospheric trace gas concentrations from polar firn and bubbly ice data by inverse methods. *J. Geophys. Res. Atmos.* **102**, 30069–30083 (1997).
244. Trudinger, C. M. et al. Modeling air movement and bubble trapping in firn. *J. Geophys. Res. Atmos.* **102**, 6747–6763 (1997).
245. Fabre, A., Barnola, J.-M., Arnaud, L. & Chappellaz, J. Determination of gas diffusivity in polar firn: comparison between experimental measurements and inverse modeling. *Geophys. Res. Lett.* **27**, 557–560 (2000).
246. Freitag, J., Dobrindt, U. & Kipfstuhl, J. A new method for predicting transport properties of polar firn with respect to gases on the pore-space scale. *Ann. Glaciol.* **35**, 538–544 (2002).
247. Trudinger, C. M. et al. How well do different tracers constrain the firn diffusivity profile? *Atmos. Chem. Phys.* **13**, 1485–1510 (2013).
248. Johnsen, S. J. et al. in *Physics of Ice Core Records*, Vol. 159 (ed. Hondoh, T.) 121–140 (Hokkaido Univ. Press, 2000).
249. Johnsen, S. J. Stable isotope homogenization of polar firn and ice. *Proc. Symp. Isot. Impurities Snow Ice* 210–219 (IAHS-AISH, 1977).
250. Jones, T. R. et al. Seasonal temperatures in West Antarctica during the Holocene. *Nature* **613**, 292–297 (2023).
251. Banwell, A. F., Wever, N., Dunmire, D. & Picard, G. Quantifying Antarctic-wide ice-shelf surface melt volume using microwave and firn model data: 1980 to 2021. *Geophys. Res. Lett.* **50**, e2023GL102744 (2023).
252. Kuipers Munneke, P. et al. Intense winter surface melt on an Antarctic Ice Shelf. *Geophys. Res. Lett.* **45**, 7615–7623 (2018).
253. Zazulie, N., Rusticucci, M. & Solomon, S. Changes in climate at high southern latitudes: a unique daily record at Orcadas spanning 1903–2008. *J. Clim.* **23**, 189–196 (2010).
254. Datta, R. T. et al. The effect of foehn-induced surface melt on firn evolution over the Northeast Antarctic Peninsula. *Geophys. Res. Lett.* **46**, 3822–3831 (2019).
255. Kuipers Munneke, P., Ligtenberg, S. R. M., Van Den Broeke, M. R. & Vaughan, D. G. Firn air depletion as a precursor of Antarctic ice-shelf collapse. *J. Glaciol.* **60**, 205–214 (2014).
256. Clem, K. R. & Raphael, M. N. Antarctica and the Southern Ocean. *State of the Climate in 2022. Bull. Am. Meteor. Soc.* **104** (Special Online Suppl.) S322–S365 (2023).
257. Hörhold, M. et al. Modern temperatures in central–north Greenland warmest in past millennium. *Nature* **613**, 503–507 (2023).
258. Culberg, R., Schroeder, D. M. & Chu, W. Extreme melt season ice layers reduce firn permeability across Greenland. *Nat. Commun.* **12**, 2336 (2021).
259. Harper, J., Saito, J. & Humphrey, N. Cold season rain event has impact on Greenland's firn layer comparable to entire summer melt season. *Geophys. Res. Lett.* **50**, e2023GL103654 (2023).
260. Kittel, C. et al. Diverging future surface mass balance between the Antarctic ice shelves and grounded ice sheet. *Cryosphere* **15**, 1215–1236 (2021).
261. Trusel, L. D. et al. Divergent trajectories of Antarctic surface melt under two twenty-first-century climate scenarios. *Nat. Geosci.* **8**, 927–932 (2015).
262. Donat-Magnin, M. et al. Future surface mass balance and surface melt in the Amundsen sector of the West Antarctic ice sheet. *Cryosphere* **15**, 571–593 (2021).
263. Gilbert, E. & Kittel, C. Surface melt and runoff on Antarctic ice shelves at 1.5°C, 2°C, and 4°C of future warming. *Geophys. Res. Lett.* **48**, e2020GL091733 (2021).
264. van Wessem, J. M., van den Broeke, M. R., Wouters, B. & Lhermitte, S. Variable temperature thresholds of melt pond formation on Antarctic ice shelves. *Nat. Clim. Change* **13**, 161–166 (2023).
265. Leeson, A. A. et al. Supraglacial lakes on the Greenland ice sheet advance inland under warming climate. *Nat. Clim. Change* **5**, 51–55 (2015).
266. Flowers, G. E. Hydrology and the future of the Greenland ice sheet. *Nat. Commun.* **9**, 2729 (2018).
267. Ashmore, D. W., Mair, D. W. F. & Burgess, D. O. Meltwater percolation, impermeable layer formation and runoff buffering on Devon Ice Cap, Canada. *J. Glaciol.* **66**, 61–73 (2020).
268. Samimi, S., Marshall, S. J. & MacFerrin, M. Meltwater penetration through temperate ice layers in the percolation zone at DYE-2, Greenland ice sheet. *Geophys. Res. Lett.* **47**, e2020GL089211 (2020).

269. Samimi, S., Marshall, S. J., Vandecrux, B. & MacFerrin, M. Time-domain reflectometry measurements and modeling of firn meltwater infiltration at DYE-2, Greenland. *J. Geophys. Res. Earth Surf.* **126**, e2021JF006295 (2021).
270. Hulbe, C. L. & Whillans, I. M. A method for determining ice-thickness change at remote locations using GPS. *Ann. Glaciol.* **20**, 263–268 (1994).
271. Hamilton, G. S., Whillans, I. M. & Morgan, P. J. First point measurements of ice-sheet thickness change in Antarctica. *Ann. Glaciol.* **27**, 125–129 (1998).
272. MacFerrin, M. J., Stevens, C. M., Vandecrux, B., Waddington, E. D. & Abdalati, W. The Greenland firn compaction verification and reconnaissance (FirnCover) dataset, 2013–2019. *Earth Syst. Sci. Data* **14**, 955–971 (2022).
273. Nicholls, K. W. et al. A ground-based radar for measuring vertical strain rates and time-varying basal melt rates in ice sheets and shelves. *J. Glaciol.* **61**, 1079–1087 (2015).
274. Katsushima, T., Adachi, S., Yamaguchi, S., Ozeki, T. & Kumakura, T. Nondestructive three-dimensional observations of flow finger and lateral flow development in dry snow using magnetic resonance imaging. *Cold Reg. Sci. Technol.* **170**, 102956 (2020).
275. Charalampidis, C. et al. Thermal tracing of retained meltwater in the lower accumulation area of the southwestern Greenland ice sheet. *Ann. Glaciol.* **57**, 1–10 (2016).
276. Webb, R. W., Jennings, K., Finsterle, S. & Fassnacht, S. R. Two-dimensional liquid water flow through snow at the plot scale in continental snowpacks: simulations and field data comparisons. *Cryosphere* **15**, 1423–1434 (2021).
277. Smith, B. E. et al. Evaluating Greenland surface-mass-balance and firn-densification data using ICESat-2 altimetry. *Cryosphere* **17**, 789–808 (2023).
278. Phan, X. V. et al. 1D-Var multilayer assimilation of X-band SAR data into a detailed snowpack model. *Cryosphere* **8**, 1975–1987 (2014).
279. Verjans, V. et al. Bayesian calibration of firn densification models. *Cryosphere* **14**, 3017–3032 (2020).
280. Prieur, C., Rabatel, A., Thomas, J.-B., Farup, I. & Chanussot, J. Machine learning approaches to automatically detect glacier snow lines on multi-spectral satellite images. *Remote. Sens.* **14**, 3868 (2022).
281. Wang, X. et al. A review of image super-resolution approaches based on deep learning and applications in remote sensing. *Remote. Sens.* **14**, 5423 (2022).
282. Hu, Z., Sun, Y., Kuipers Munneke, P., Lhermitte, S. & Zhu, X. Towards a spatially transferable super resolution model for downscaling Antarctic surface melt. In *NeurIPS 2022 Workshop on Tackling Climate Change with Machine Learning* (Climate Change AI, 2022).
283. Rizzoli, P., Martone, M., Rott, H. & Moreira, A. Characterization of snow facies on the Greenland ice sheet observed by TanDEM-X interferometric SAR data. *Remote. Sens.* **9**, 315 (2017).
284. Dell, R. L. et al. Supervised classification of slush and ponded water on Antarctic ice shelves using Landsat 8 imagery — Corrigendum. *J. Glaciol.* **68**, 415–416 (2022).
285. Dunmire, D., Banwell, A. F., Wever, N., Lenaerts, J. T. M. & Datta, R. T. Contrasting regional variability of buried meltwater extent over 2 years across the Greenland ice sheet. *Cryosphere* **15**, 2983–3005 (2021).
286. Reichstein, M. et al. Deep learning and process understanding for data-driven Earth system science. *Nature* **566**, 195–204 (2019).
287. Medley, B., Lenaerts, J. T. M., Dattler, M., Keenan, E. & Wever, N. Predicting Antarctic net snow accumulation at the kilometer scale and its impact on observed height changes. *Geophys. Res. Lett.* **49**, e2022GL099330 (2022).
288. Montgomery, L., Koenig, L. & Alexander, P. The SUMup dataset: compiled measurements of surface mass balance components over ice sheets and sea ice with analysis over Greenland. *Earth Syst. Sci. Data* **10**, 1959–1985 (2018).
289. Essery, R., Morin, S., Lejeune, Y. & Ménard, B. C. A comparison of 1701 snow models using observations from an alpine site. *Adv. Water Resour.* **55**, 131–148 (2013).
290. Levermann, A. & Winkelmann, R. A simple equation for the melt elevation feedback of ice sheets. *Cryosphere* **10**, 1799–1807 (2016).
291. Kuiper, E.-J. N. et al. Using a composite flow law to model deformation in the NEEM deep ice core, Greenland — Part 2: The role of grain size and premelting on ice deformation at high homologous temperature. *Cryosphere* **14**, 2449–2467 (2020).
292. Schneider, A. M., Zender, C. S. & Price, S. F. More realistic intermediate depth dry firn densification in the energy exascale Earth System Model (E3SM). *J. Adv. Model. Earth Syst.* **14**, e2021MS002542 (2022).
293. Lambin, C., Fettweis, X., Kittel, C., Fonder, M. & Ernst, D. Assessment of future wind speed and wind power changes over south Greenland using the Modèle Atmosphérique Régional regional climate model. *Int. J. Climatol.* **43**, 558–574 (2022).
294. Fretwell, P. et al. Bedmap2: improved ice bed, surface and thickness datasets for Antarctica. *Cryosphere* **7**, 375–393 (2013).
295. Johnson, A., Hock, R. & Fahnestock, M. Spatial variability and regional trends of Antarctic ice shelf surface melt duration over 1979–2020 derived from passive microwave data. *J. Glaciol.* **68**, 533–546 (2022).
296. Das, I. et al. Influence of persistent wind scour on the surface mass balance of Antarctica. *Nat. Geosci.* **6**, 367–371 (2013).
297. Hui, F. et al. Mapping blue-ice areas in Antarctica using ETM+ and MODIS data. *Ann. Glaciol.* **55**, 129–137 (2014).
298. Morlighem, M. et al. BedMachine v3: complete bed topography and ocean bathymetry mapping of Greenland from multibeam echo sounding combined with mass conservation. *Geophys. Res. Lett.* **44**, 11051–11061 (2017).
299. Ryan, J. C. et al. Greenland ice sheet surface melt amplified by snowline migration and bare ice exposure. *Sci. Adv.* **5**, eaav3738 (2019).
300. Zheng, L. et al. Greenland ice sheet daily surface melt flux observed from space. *Geophys. Res. Lett.* **49**, e2021GL096690 (2022).

## Acknowledgements
This Review is the result of the International Firn Symposium held online in June 2022, which was intentionally collaborative and inclusive in its setup. No travel or participation expenses were required. Junior and senior scientists were paired for writing the sections. As such, this paper is written as a team effort without a specified author order. We thank all symposium participants for their contributions and discussions. We also thank K. Poinar for her feedback on the representation of hydrological features in Fig. 1.

## Author contributions
P.K.M. led the Introduction. C.A., N.H. and R.T.D. led 'Atmospheric forcing'. I.McD. and C.M.S. led 'Firn properties'. R.C. and C.M. led 'Firn hydrology'. R.De., D.Ma., D.Mo., E.R.T., R.Dr., E.P., S.S., S.deR.H., C.B., C.E. and K.K. led 'Firn observations'. A.H., E.M., F.M.O. and T.S. led 'Modelling dry firn densification'. S.B. and J.M. led 'Modelling wet firn and firn hydrology'. C.B. led 'Modelling chemical tracer transport'. C.A. and R.T.D. led 'The changing ice-sheet and ice-shelf firn'. E.C., D.D., S.L., N.-J.S., M.T.-M., N.W. and B.W. led the 'Summary and future perspectives'. N.C. and A.K. contributed to earlier drafts of the manuscript. Figs. 1 and 3 were created by R.T.D., Figs. 2 and 6 by C.A., Fig. 4 by R.C., and Fig. 5 by S.deR.H. J.T.M.L. and N.W. coordinated the International Firn Symposium that resulted in this Review. R.T.D, P.K.M. and N.W. coordinated the paper writing and did the final editing.

## Competing interests
The authors declare no competing interests.

## Additional information
**Peer review information** *Nature Reviews Earth & Environment* thanks Baptiste Vandecrux, Vincent Verjans and the other, anonymous, reviewer(s) for their contribution to the peer review of this work.



## The Firn Symposium team

**Charles Amory [1], Christo Buizert [2], Sammie Buzzard [3,4], Elizabeth Case [5], Nicole Clerx [6], Riley Culberg [7], Rajashree Tri Datta [8], Rahul Dey [9], Reinhard Drews [10], Devon Dunmire [8], Clare Eayrs [11,12], Nicolaj Hansen [13,14], Angelika Humbert [15,16], Athul Kaitheri [17], Kaitlin Keegan [18], Peter Kuipers Munneke [19], Jan T. M. Lenaerts [8], Stef Lhermitte [20,21], Doug Mair [22], Ian McDowell [18,23], Jessica Mejia [24], Colin R. Meyer [25], Elizabeth Morris [26], Dorothea Moser [27,28], Falk M. Oraschewski [10], Emma Pearce [29], Sophie de Roda Husman [21], Nicole-Jeanne Schlegel [30,31], Timm Schultz [32], Sebastian B. Simonsen [13], C. Max Stevens [33,34], Elizabeth R. Thomas [27], Megan Thompson-Munson [8,35], Nander Wever [8,36] ✉ & Bert Wouters [21]**

[1]Institut des Géosciences de l'Environnement, University Grenoble Alpes, CNRS, Grenoble, France. [2]College of Earth, Ocean and Atmospheric Sciences, Oregon State University, Corvallis, OR, USA. [3]School of Earth and Environmental Sciences, Cardiff University, Cardiff, UK. [4]Department of Geography and Environmental Sciences, Northumbria University, Newcastle upon Tyne, UK. [5]Department of Earth and Environmental Sciences, Columbia University, NY, USA. [6]Department of Geosciences, Université de Fribourg, Fribourg, Switzerland. [7]Department of Earth and Atmospheric Sciences, Cornell University, Ithaca, NY, USA. [8]Department of Atmospheric and Oceanic Sciences, University of Colorado Boulder, Boulder, CO, USA. [9]National Centre for Polar and Ocean Research (NCPOR), Ministry of Earth Sciences, Vasco da Gama, Goa, India. [10]Department of Geosciences, University of Tübingen, Tübingen, Germany. [11]Center for Global Sea Level Change, New York University Abu Dhabi, Abu Dhabi, UAE. [12]Department of Glacial Environment Research, Korea Polar Research Institute, Incheon, Republic of Korea. [13]Geodesy and Earth Observation, DTU Space, Technical University of Denmark, Kongens Lyngby, Denmark. [14]Danish Meteorological Institute, Copenhagen, Denmark. [15]Alfred Wegener Institute Helmholtz Centre for Polar and Marine Research, Bremerhaven, Germany. [16]Faculty of Geosciences, University of Bremen, Bremen, Germany. [17]Observatoire de la Côte d'Azur, Université Côte d'Azur, CNRS, Valbonne, France. [18]Department of Geological Sciences and Engineering, University of Nevada, Reno, USA. [19]Institute for Marine and Atmospheric Research (IMAU), Utrecht University, Utrecht, The Netherlands. [20]Department of Earth and Environmental Sciences, KU Leuven, Leuven, Belgium. [21]Department of Geoscience and Remote Sensing, Delft University of Technology (TUDelft), Delft, The Netherlands. [22]School of Environmental Sciences, University of Liverpool, Liverpool, UK. [23]Graduate Program of Hydrologic Sciences, University of Nevada, Reno, NV, USA. [24]Department of Geology, University at Buffalo, Buffalo, NY, USA. [25]Thayer School of Engineering, Dartmouth College, Hanover, NH, USA. [26]Scott Polar Research Institute, University of Cambridge, Cambridge, UK. [27]Ice Dynamics and Palaeoclimate, British Antarctic Survey, Cambridge, UK. [28]Department of Earth Sciences, University of Cambridge, Cambridge, UK. [29]Institut Terre et Environnement de Strasbourg (ITES), Université de Strasbourg, Strasbourg, France. [30]Jet Propulsion Laboratory, California Institute of Technology, Pasadena, CA, USA. [31]NOAA Geophysical Fluid Dynamics Laboratory, Princeton, NJ, USA. [32]Institute for Mechanics, TU Darmstadt, Darmstadt, Germany. [33]Earth System Science Interdisciplinary Center, University of Maryland, College Park, MD, USA. [34]Cryospheric Sciences Laboratory, NASA Goddard Space Flight Center, Greenbelt, MD, USA. [35]Cooperative Institute for Research in Environmental Sciences (CIRES), University of Colorado Boulder, Boulder, CO, USA. [36]WSL Institute for Snow and Avalanche Research SLF, Davos, Switzerland.